PASJ: Publ. Astron. Soc. Japan **63**, 763–794, 2011 August 25

Sagittarius A Molecular Cloud Complex in $H^{13}CO^+$ and Thermal SiO Emission Lines

Masato TSUBOI and Ken-ichi TADAKI
Institute of Space and Astronautical Science, 3-1-1 Yoshinodai, Chuou-ku, Sagamihara 252-5210
Department of Astronomy, The University of Tokyo, 7-3-1 Hongo, Bunkyo, Tokyo 113-0033
tsuboi@vsop.isas.jaxa.jp
Atsushi MIYAZAKI
Mizusawa VLBI Observatory, National Astronomical Observatory, Mizusawa, Oshu, Iwate 023-0861
and
Toshihiro HANDA
Institute of Astronomy, The University of Tokyo, 2-21-1 Osawa, Mitaka, Tokyo 181-0015

(Received 2010 October 4; accepted 2011 April 11)

Abstract

We present results of a high-resolution wide-field mapping observation of the Sagittarius A (Sgr A) molecular cloud complex in $H^{13}CO^+$ $J = 1$–0 and thermal SiO $J = 2$–1 emission lines with the 25-beam receiver of the 100 GHz band operating on the Nobeyama Radio Observatory 45-m telescope. The mapping area covers a $0\overset{\circ}{.}5 \times 0\overset{\circ}{.}5$ area involving several named molecular clouds, for example GCM −0.02−0.07, GCM −0.13−0.08, GCM 0.11−0.11, the Sickle molecular cloud, the Arched filaments molecular cloud, and so on. The data have an effective angular resolution of $26''$. The $H^{13}CO^+$ emission line is a famous tracer of molecular gas mass because the line is optically thin, even in the Galactic center region, and is not emphasized by shock. The emission line presents a clumpy distribution of the molecular cloud. The averaged fractional abundance in the Sgr A complex is $N(H^{13}CO^+)/N_{H_2} \simeq (1.8 \pm 0.4) \times 10^{-11}$, comparing the LTE mass and the virial theorem mass. The SiO emission line is a famous and reliable tracer of shocked molecular gas. We find many molecular clouds that are remarkable only in the SiO emission line. Such molecular clouds have a large velocity width of up to 60 km s^{-1}. The brightness temperature ratio is up to $T_B(\mathrm{SiO})/T_B(H^{13}CO^+) \lesssim 8$. The features are dominated by shock SiO-enriched gas. In such clouds, the ratio of the fractional abundance of SiO and $H^{13}CO^+$ molecules is $X(\mathrm{SiO})/X(H^{13}CO^+) \sim 100$. The features are presumably made by supernova remnants. We found a prototypical example in GCM −0.02−0.07. It has two distinct structures. One is a ridge-like structure contacting with the Sgr A East shell; another is an expanding shell-like structure. There is a wide-velocity width ridge of SiO-enriched gas in GCM 0.11−0.11, which is adjacent to Vertical filaments. This suggests that the collision with the molecular cloud accelerates relativistic electrons, which illuminate the Vertical filaments–Polarized Plumes complex.

Key words: Galaxy: center — ISM: clouds — ISM: magnetic fileds — ISM: supernova remnants

1. Introduction

The Galactic center region is the nearest nucleus of a spiral galaxy. The counterpart of central molecular cloud condensation often observed in nearby spiral galaxies is observed in this region as the Central Molecular Zone (CMZ) (Morris & Serabyn 1996). The CMZ involves fascinating features associated with star formation fed by molecular clouds infalling to the Galactic center region. Although similar features will be observed in the central regions in nearby spiral galaxies with further giant radio telescopes, we can observe them in the CMZ using the present radio telescopes. This point view is one of the advantages of Galactic center observations.

The Sagittarius A (Sgr A) molecular cloud complex involves several massive molecular gas condensations, for example the 50-km s^{-1} molecular cloud (GCM −0.02−0.07), the 20-km s^{-1} molecular cloud (GCM −0.13−0.08), the GCM 0.11−0.11 molecular cloud, the Sickle molecular cloud, the Arched filaments molecular cloud, and so on. CO and CS lines are useful for structure finding in the CMZ (e.g., Bally et al. 1987; Oka et al. 1998; Tsuboi et al. 1999). The appearances in CO and CS lines of these molecular clouds resemble each other, although the critical densities of these lines are significantly different (CO: 10^2 cm^{-3}, CS: 10^5 cm^{-3}). The cause is that CO and CS lines are sensitive both for the molecular cloud, itself, and shocked molecular gas. They presumably become optically thick easily, even at the cloud surface or geometrically thin shocked gas. This characteristic is a disadvantage for quantitative analysis of the distribution of molecular gas and the total molecular mass in the molecular cloud. An optically thin line is suitable for quantitative analysis. Because there is no optically thin molecular line with a strong brightness temperature, it has been hard to observe them. However, recent technical improvements in the sensitivity of radio telescopes provide a new possibility of observations of such weak emission lines.

The $H^{13}CO^+$ line is expected to be optically thin, even in the Sgr A molecular cloud complex, because of its small abundance; also, this line is not emphasized by shock (e.g., Handa et al. 2006). The distribution usually resembles that of the submm continuum in the disk region of the Galaxy. Thus, the

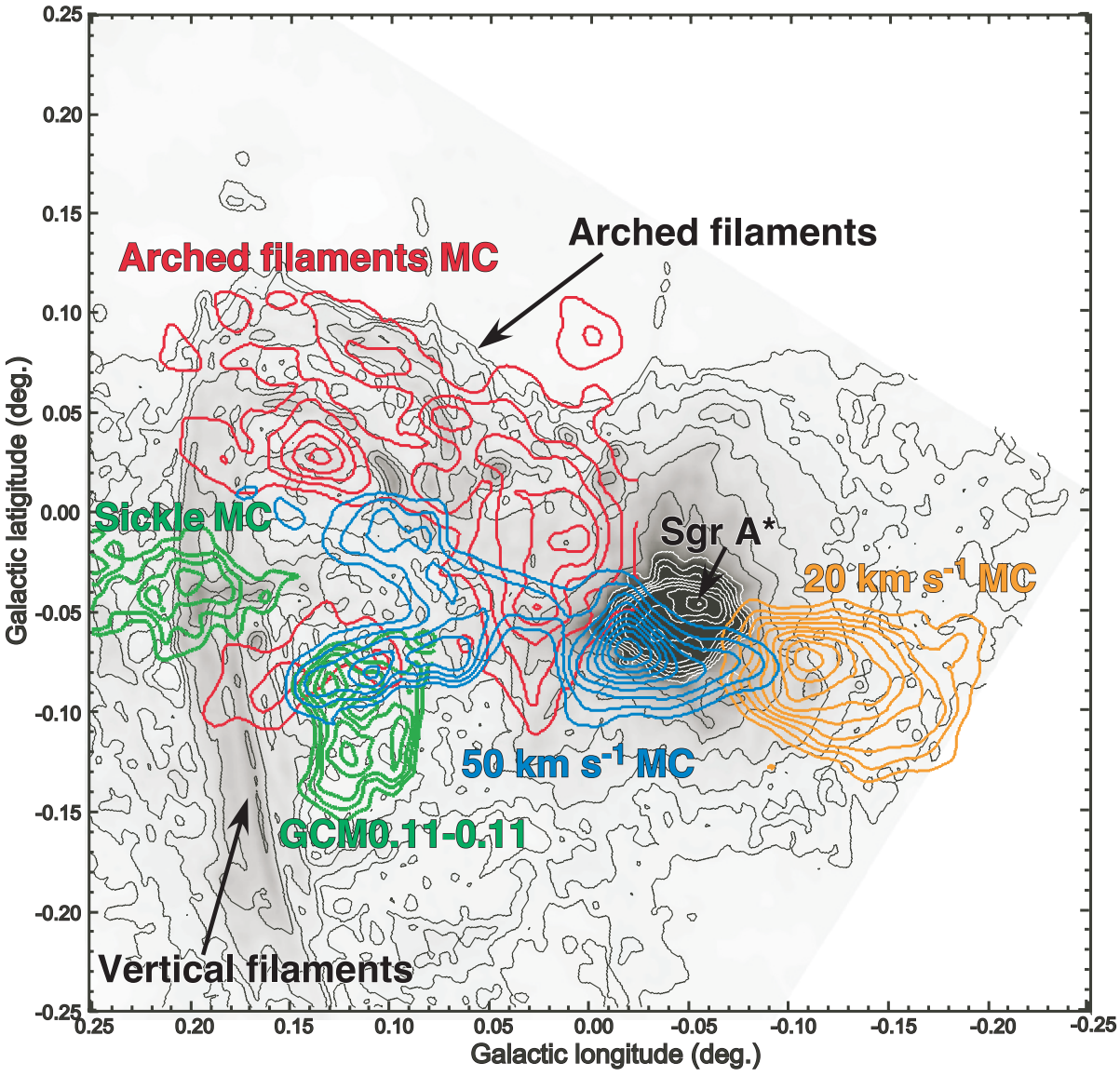

Fig. 1. Finding chart of named molecular clouds in the Sgr A region. The molecular clouds identified in CS $J = 1$–0 emission (Tsuboi et al. 1999) are superimposed on the continuum map at 20 cm (gray scale; Yusef-Zadeh et al. 1984). Red contours show the Arched filaments molecular cloud in the velocity range of −30–0 km s^{-1}. Orange contours show the 20-km s^{-1} molecular cloud (GCM −0.13−0.08) in the velocity range of 0–30 km s^{-1}. Green contours show GCM 0.11−0.11 and the Sickle molecular cloud in the velocity range of 15–45 km s^{-1}. And blue contours show the 50 km s^{-1} molecular cloud (GCM −0.02−0.07) in the velocity range of 30–60 km s^{-1}.

$H^{13}CO^+$ $J = 1$–0 line is a good tracer of molecular gas mass. A quantitative estimation of mass of the molecular cloud in the Galactic center region requires mapping observations of the $H^{13}CO^+$ emission line. In addition, the thermal SiO $J = 2$–1 emission line is located only 93 MHz from the $H^{13}CO^+$ $J = 1$–0 line. As is well known, this line is a famous and reliable tracer of shocked molecular gas (Ziurys et al. 1989). High-resolution imaging in the thermal SiO emission line provides useful information to add to our understanding of shocked gas in the Galactic center molecular cloud. Detailed observations and their correlation between $H^{13}CO^+$ and SiO emission line properties should provide unprecedented information about the Galactic center molecular cloud. In addition, the comparison in the SiO $v = 0$, $J = 2$–1 and $H^{13}CO^+$ lines of external galaxies had been studied so as to explore the physical conditions of molecular gas actively, since SiO emissions were first detected in NGC 253 (Mauersberger & Henkel 1991).

In this paper, we present observations of the Sgr A molecular cloud comlex in the $H^{13}CO^+$ $J = 1$–0 and SiO $v = 0$, $J = 2$–1 emission lines using the Nobeyama Radio Observatory (NRO)[1] 45-m telescope in order to obtain the mass distribution of the molecular clouds, and to explore the shock-induced structures with higher angular resolution. Throughout this paper, we adopt 8.5 kpc as the distance of the Galactic center. In addition, we use Galactic coordinates.

[1] Nobeyama Radio Observatory is a branch of National Astronomical Observatory, National Institutes of Natural Sciences, Japan.

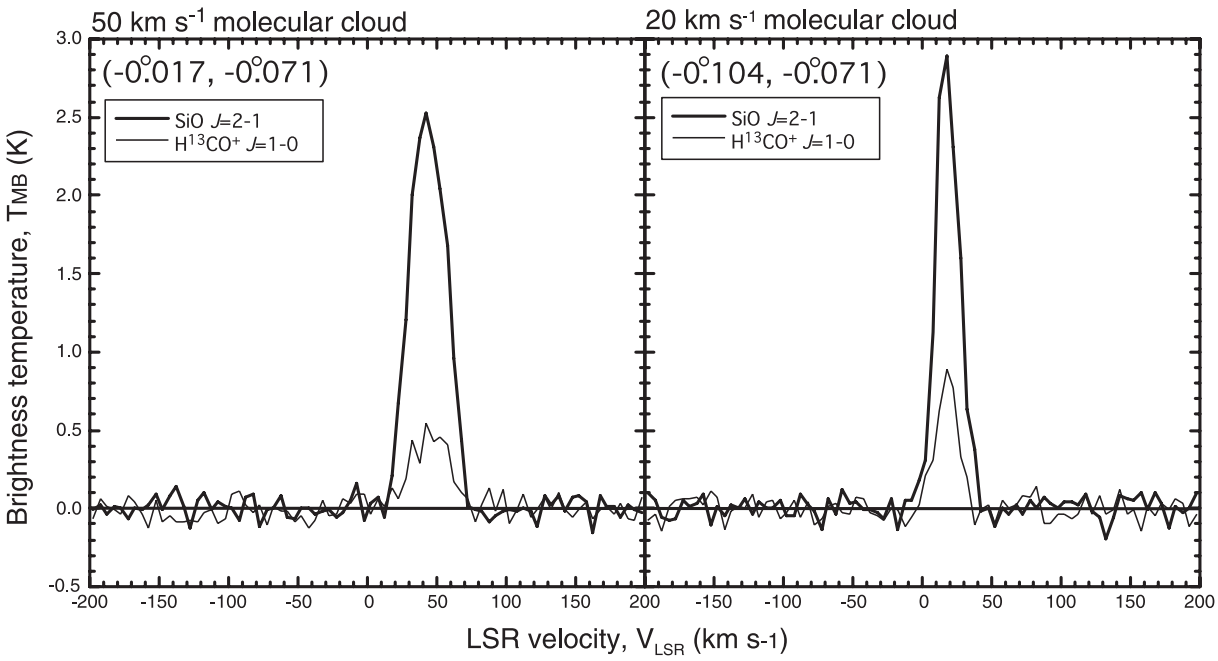

Fig. 2. Typical spectra on the 50 km s^{-1} molecular cloud (left panel) and the 20 km s^{-1} molecular cloud (right panel). The observed positions are shown on the upper-left corner of each panel. The brightness temperature ratios of these positions are $T_{\rm B}({\rm SiO})/T_{\rm B}({\rm H^{13}CO^+}) \sim 5$ and 3, respectively.

2. Observations

2.1. *On-The-Fly Observations in SiO $v = 0$, $J = 2$–1, and $H^{13}CO^+$ $J = 1$–0 Emission Lines*

We performed simultaneous observations of the Sgr A molecular cloud in the $H^{13}CO^+$ $J = 1$–0 ($\nu = 86.754330$ GHz) and SiO $v = 0$, $J = 2$–1 ($\nu = 86.847010$ GHz) lines with the 45-m radio telescope of NRO in 2007 February and March. The observation area was a square of $0.^\circ5 \times 0.^\circ5$, centered at $l = 0^\circ$, $b = 0^\circ$. The area includes Arched filaments, the GCM 0.11−0.11 molecular cloud, the 50-km s^{-1} molecular cloud, and the 20-km s^{-1} molecular cloud (see figure 1).

We used the 25-beam (5 × 5) SIS receiver (BEARS) of the 100 GHz band installed in the NRO 45-m telescope (Sunada et al. 2000). The observations were performed during a survey program of the Galactic center region with BEARS in the $H^{13}CO^+$ and SiO emission lines. The full width half maximum (FWHM) of the 45-m telescope beam was 20″ at 86 GHz. At the Galactic center distance of 8.5 kpc, the beam size corresponds to about 0.8 pc. The typical aperture efficiency and the main beam efficiency were 40% and 50% at 86 GHz. The typical system temperature during the observations was about 300 K (DSB). The mapping mode was the On-The-Fly observation mode (Sawada et al. 2008). The scan interval was 7″, which corresponds to one third of the telescope beam. As backend spectrometers, we used digital auto-correlators which covered an instantaneous bandwidth of about 512 MHz with a spectral resolution of 500 kHz, with 1024 channels. These correspond to about 1740 km s^{-1} for the velocity coverage and 1.8 km s^{-1} for the velocity resolution, respectively. We simultaneously observed $H^{13}CO^+$ $J = 1$–0 and SiO $v = 0$, $J = 2$–1 emission lines. The frequency separation of both lines was 93 MHz, as mentioned previously, which corresponds to velocity difference of 320 km s^{-1}. There may be a blend between the extreme positive velocity component (≥ 160 km s^{-1}) of SiO and the extreme negative velocity component (≤ -160 km s^{-1}) of $H^{13}CO^+$. However, the fraction of molecular clouds with velocity extent over ± 160 km s^{-1} was quite small, even in the Sgr A molecular cloud. Thus, the blend of these emission lines should not be critical. Typical spectra on the 50-km s^{-1} molecular cloud and the 20-km s^{-1} molecular cloud are shown in figure 2.

All spectra were obtained by On-The-Fly mapping with an off position of about $1.^\circ0$ in the direction of the Galactic latitude. The intensity scale of the spectra was calibrated using the chopper wheel method in order to correct the antenna temperature for atmospheric attenuation, $T_{\rm A}^*$ (SSB). The data were reduced on the NEWSTAR reduction package of NRO. We subtracted the baselines of the spectra by fitting linear lines or, if necessary, low-degree polynomials that produce flat baselines in emission-free velocity ranges.

Then, all spectra were scaled so that the line intensity of some reference positions became the same as those observed by the single-beam receiver with an image-rejection filter, S100, in order to compensate for the imperfect image rejection ratio of BEARS. The typical achieved r.m.s. noise of the spectra was 0.035 K/5 km s^{-1} in $T_{\rm A}^*$ (SSB). Pointing errors were corrected about every 2.5 hr by observing a strong SiO maser source, VX Sgr or OH 2.6−0.4, with a 40-GHz band receiver. The typical pointing accuracy was 5″ during the observation.

2.2. *SiO $v = 0$, $J = 1$–0 Observations*

We additionally performed an observation of the Sgr A molecular cloud in SiO $v = 0$, $J = 1$–0 ($\nu = 43.4238$ GHz) line with the 45-m radio telescope. The observation area included

the 50-km s^{-1} molecular cloud and the 20-km s^{-1} molecular cloud, but did not include an area with $b > -2'$. We used a single-beam SIS receiver of the 40 GHz band with an image rejection filter. The aperture efficiency and the main beam efficiency were 60% and 70% at 43 GHz. The FWHM of the 45-m telescope beam was 40″ at 43 GHz. The sampling grid spacing was 20″, which corresponds to Nyquist sampling. The typical system temperature during the observations was about 220 K (SSB). As backend spectrometers, we used wide-band acousto-optical spectrometers (AOS-W). All spectra were obtained by position switching with an off position of about 1°.0 in the direction of the Galactic latitude. The intensity scale of the spectra was calibrated using the chopper wheel method in order to correct the antenna temperature for atmospheric attenuation, $T_{\rm A}^*$ (SSB). The data were reduced on the NEWSTAR reduction package of NRO. Baseline subtractions were done using the same procedures as mentioned above. The typical achieved r.m.s. noise of the spectra was 0.07 K/5 km s^{-1} in $T_{\rm A}^*$ (SSB). Pointing errors were corrected about every 2 hr by observing a strong SiO maser source, AH Sco, with the same receiver. The typical pointing accuracy was less than 5″ during the observation.

3. Results

Figure 3 and figure 4 show velocity channel maps of the Sgr A molecular cloud complex in the SiO $v = 0$, $J = 2$–1, and $H^{13}CO^+$ $J = 1$–0 emission lines, respectively. The data gird is 7″ × 7″. The resultant angular resolution in the maps is 26″ after smoothing with a Gaussian weighting function. This corresponds to about 1 pc at the Galactic center distance. The velocity integrated width is 10 km s^{-1}. Galactic center molecular clouds in these lines are both identified from $V_{\rm LSR} = -50$ to 125 km s^{-1}. There is no statistically significant feature with velocities outside this range. The molecular clouds in the $H^{13}CO^+$ emission line are clumpy compared with that of previous molecular line observations. Some molecular clouds are resolved into several filaments in the channel maps. We compared the distributions in channel maps of these molecular lines, and found many molecular clouds visible only in the SiO emission line. Such molecular clouds have a large velocity width of up to 60 km s^{-1}, and a high brightness temperature ratio of up to $R_{\rm SiO/H^{13}CO^+} = T_{\rm B}[{\rm SiO}(2\text{–}1)] / T_{\rm B}[{\rm H^{13}CO^+}(1\text{–}0)] \simeq 8$. A high ratio indicates that there is shocked molecular gas with physical interaction in the area. The brightness temperature ratio should provide important information about the interaction. We present some remarks in the following subsections.

Figure 5 shows velocity channel maps of the molecular clouds surrounding Sgr A in the SiO $v = 0$, $J = 1$–0 emission line. The data gird is 20″ × 20″. The resultant angular resolution in the maps is 52″ after smoothing with a Gaussian weighting function.

3.1. Arched Filaments Molecular Cloud

Arched filaments are curved filamentary ionized gas located between Sgr A and Vertical filaments (Yusef-Zadeh et al. 1984, also see figure 1). In previous observations (e.g., Serabyn & Güsten 1987; Tsuboi et al. 1999), Arched filaments have a molecular cloud counterpart in the CS emission lines (hereafter, Arched filaments molecular cloud). The morphological complementation between them suggests that this molecular cloud is interacting with Arched filaments. The molecular cloud is clearly seen from $V_{\rm LSR} = -35$ km s^{-1} to $V_{\rm LSR} = 5$ km s^{-1} in the SiO and $H^{13}CO^+$ emission lines (see figure 3 and figure 4). Figures 6a and 6b show the velocity-integrated maps of the molecular cloud in the SiO and $H^{13}CO^+$ emission lines. The integrated velocity range is $V_{\rm LSR} = -30$–0 km s^{-1}. Figure 6c shows the brightness temperature ratio of the SiO and $H^{13}CO^+$ emission lines, $R_{\rm SiO/H^{13}CO^+}$, in this velocity range. Figure 6d shows the molecular cloud in the CS $J = 1$–0 emission line (contours; Tsuboi et al. 1999) and the continuum emission at 20 cm observed by VLA (gray scale; Yusef-Zadeh & Morris 1987) for a comparison. There is another molecular cloud with a positive velocity of $V_{\rm LSR} = 35$ km s^{-1} to $V_{\rm LSR} = 65$ km s^{-1} in the same region (see figure 3 and figure 4). However, this cloud has no detailed morphological complementation for Arched filaments. The positive velocity cloud is not likely to be associated with Arched filaments.

The positive longitude half ($l \geq 0°.05$) of the Arched filaments molecular cloud consists of three arm-like structures, which are two positive-latitude curved arms extending along Arched filaments and one negative-latitude curved arm extending roughly parallel to the Galactic plane (see figures 6a and 6b). The appearances of these arms in the SiO and $H^{13}CO^+$ emission lines are clumpy, although these counterparts in CS are seen to be continuous or less lumpy. The temperature ratio in the curved arms is approximately lower than unity, $R_{\rm SiO/H^{13}CO^+} \lesssim 1$. The negative latitude arm is clearly seen in the $H^{13}CO^+$ emission line. This arm almost disappeares in the SiO emission line, except for a compact component centered at $l = 0°.17$, $b = -0°.08$. This component is probably associated with a compact continuum source on Vertical filaments (N3 in figure 3 of Yusef-Zadeh & Morris 1987). The temperature ratio at the compact component is as high as four, $R_{\rm SiO/H^{13}CO^+} \simeq 4$. This high ratio suggests that the compact component interacts physically with the continuum source. Meanwhile, the distributions of other brightness temperature ratios, $R_{\rm SiO/CS} = T_{\rm B}({\rm SiO}\ J = 2\text{–}1) / T_{\rm B}({\rm CS}\ J = 1\text{–}0)$ and $R_{\rm H^{13}CO^+/CS} = T_{\rm B}({\rm H^{13}CO^+}\ J = 1\text{–}0) / T_{\rm B}({\rm CS}\ J = 1\text{–}0)$, are fairly smooth. The ratios are $R_{\rm SiO/CS} \lesssim 0.3$ and $R_{\rm H^{13}CO^+/CS} \lesssim 0.3$.

The negative longitude half ($l \leq 0°.05$) of the Arched filaments molecular cloud is located in the "continuum gap" between Arched filaments and Sgr A. This part is clearly seen in both emission lines. There are two curved intensity ridges in the part in the SiO line. The first one is centered at $l = 0°.015$, $b = -0°.010$. This is not remarkable in the $H^{13}CO^+$ line, although there is a counterpart in the CS line. The brightness temperature ratio of the ridge is as high as four, $R_{\rm SiO/H^{13}CO^+} \simeq 4$. The second one is centered at $l = 0°.02$, $b = -0°.05$. The ridge is also remarkable in the $H^{13}CO^+$ and CS lines. The negative latitude arm mentioned above is seen to be extended from the ridge. This may also be extended to negative longitude. The ratio in the ridge is about two, $R_{\rm SiO/H^{13}CO^+} \simeq 2$. The temperature ratio in the other portion of the half is approximately lower than

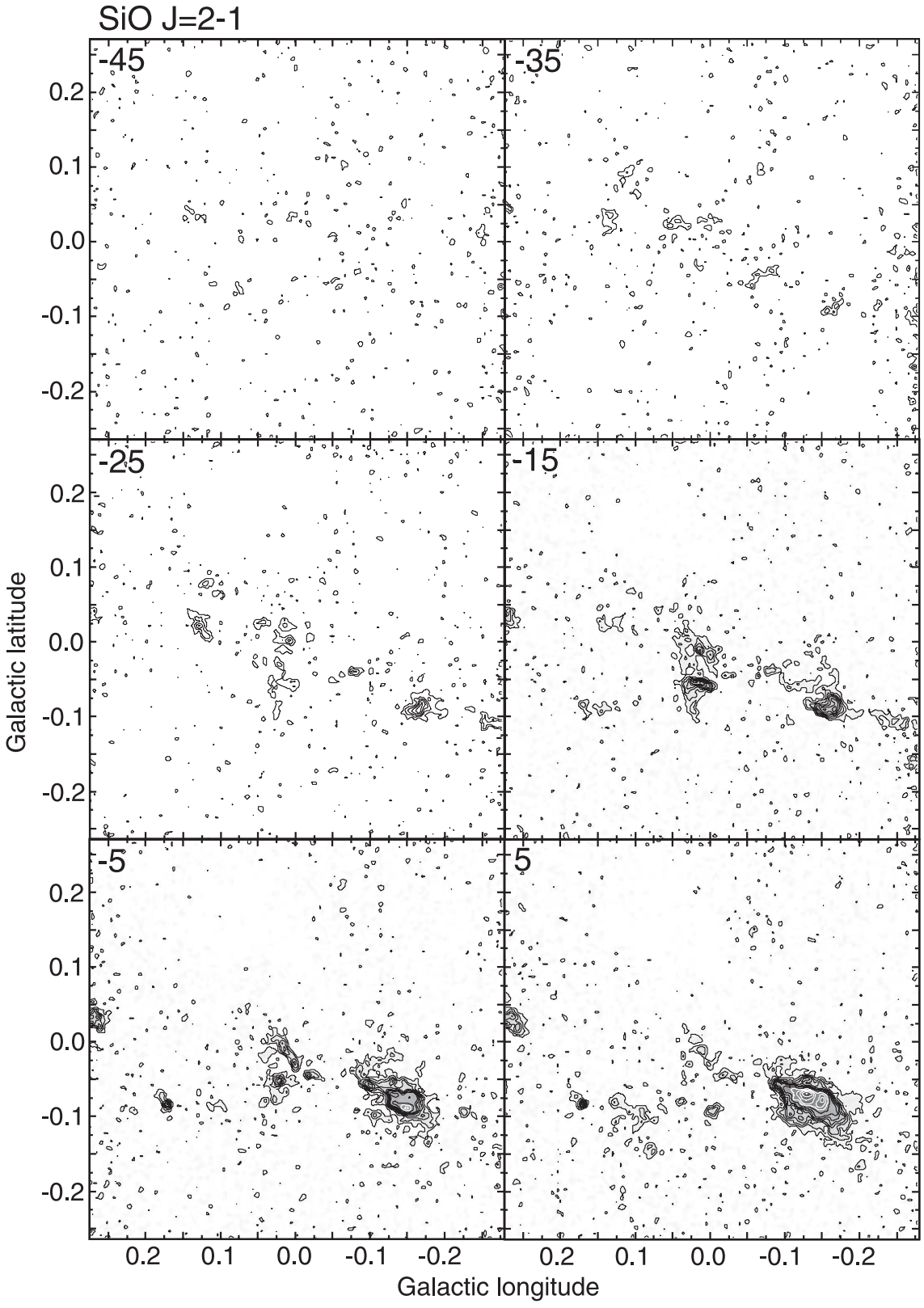

Fig. 3. Channel maps of the Sgr A molecular cloud complex in the SiO $v = 0$, $J = 2$–1 emission line. The angular resolution is FWHM $= 26''$. The velocity integrated width is $10\,\mathrm{km\,s^{-1}}$. Center velocities in V_{LSR} ($\mathrm{km\,s^{-1}}$) are shown in the upper-left corner of each map. Contour intervals are 0.159 K in 0.159–1.114 K and 0.318 K in 1.114–3.977 K in T_{MB}. The typical r.m.s. noise is 0.056 K in T_{MB}.

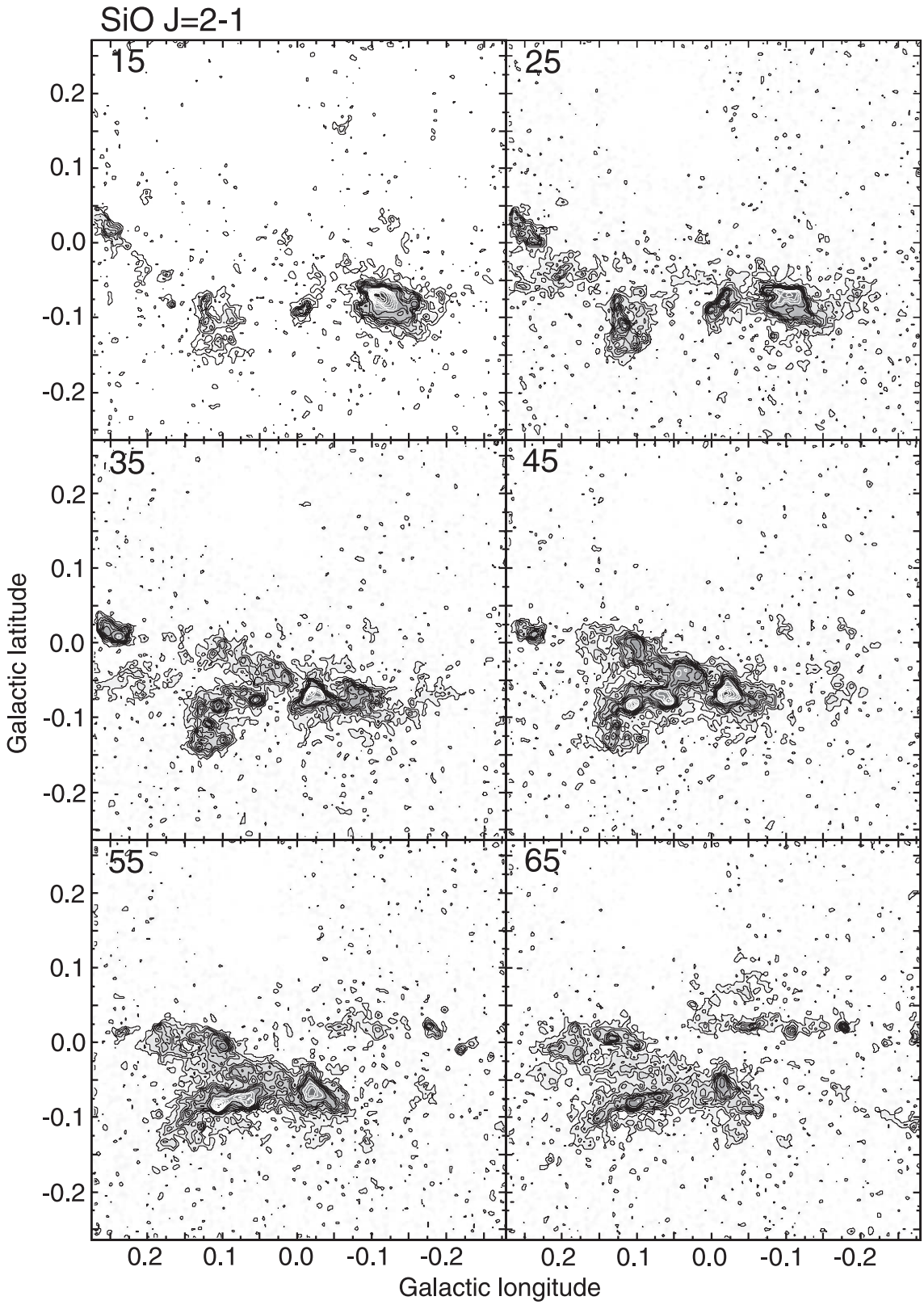

Fig. 3. (Continued)

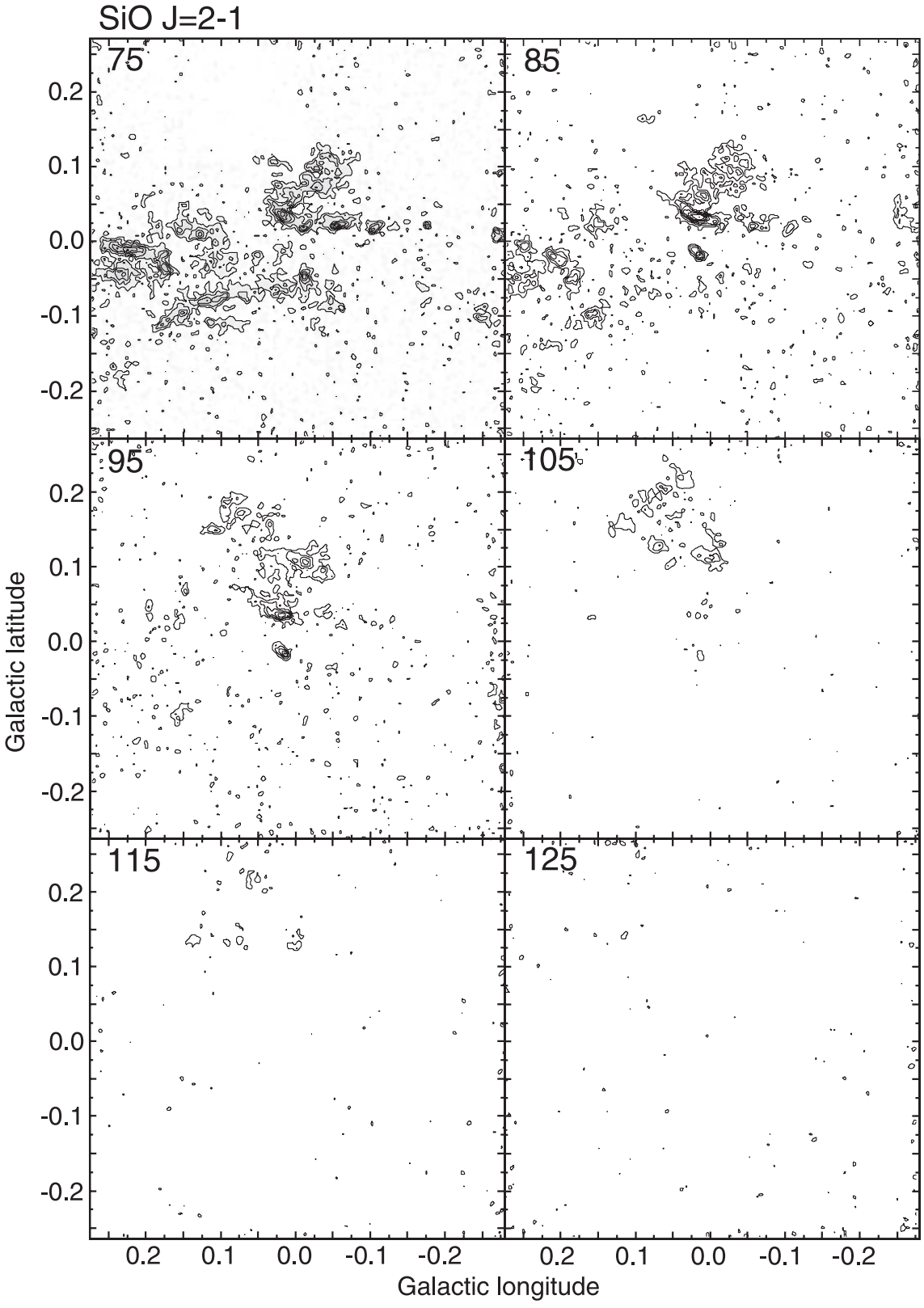

Fig. 3. (Continued)

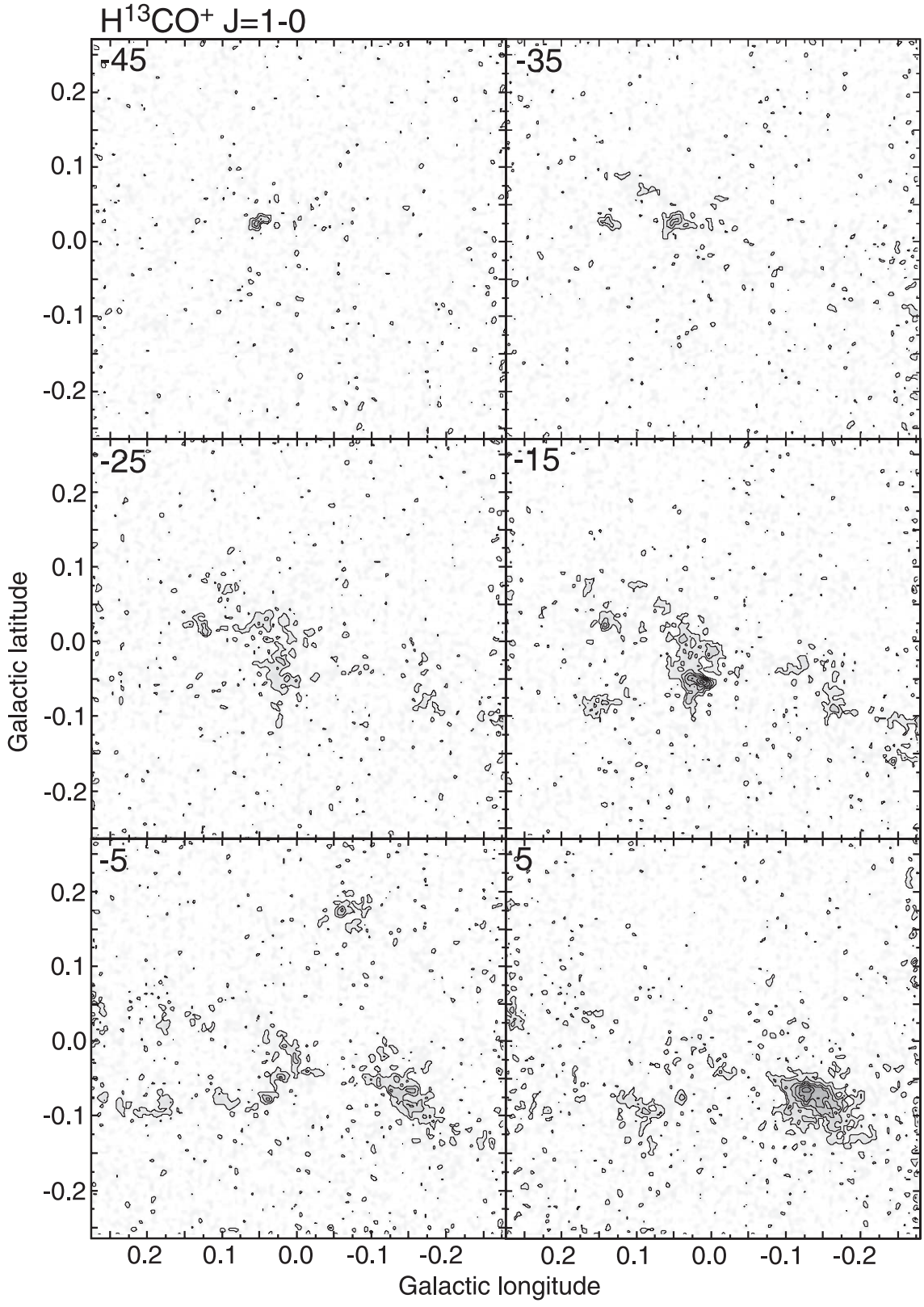

Fig. 4. Channel maps of the Sgr A molecular cloud complex in the $H^{13}CO^{+}$ $J = 1$–0 emission line. The angular resolution is FWHM $= 26''$. The velocity integrated width is $10\,\mathrm{km\,s^{-1}}$. Center velocities in V_{LSR} ($\mathrm{km\,s^{-1}}$) are shown in the upper-left corner of each map. The first contour and contour level are both $T_{\mathrm{MB}} = 0.159$ K. The typical noise level in the map is 0.056 K in T_{MB}.

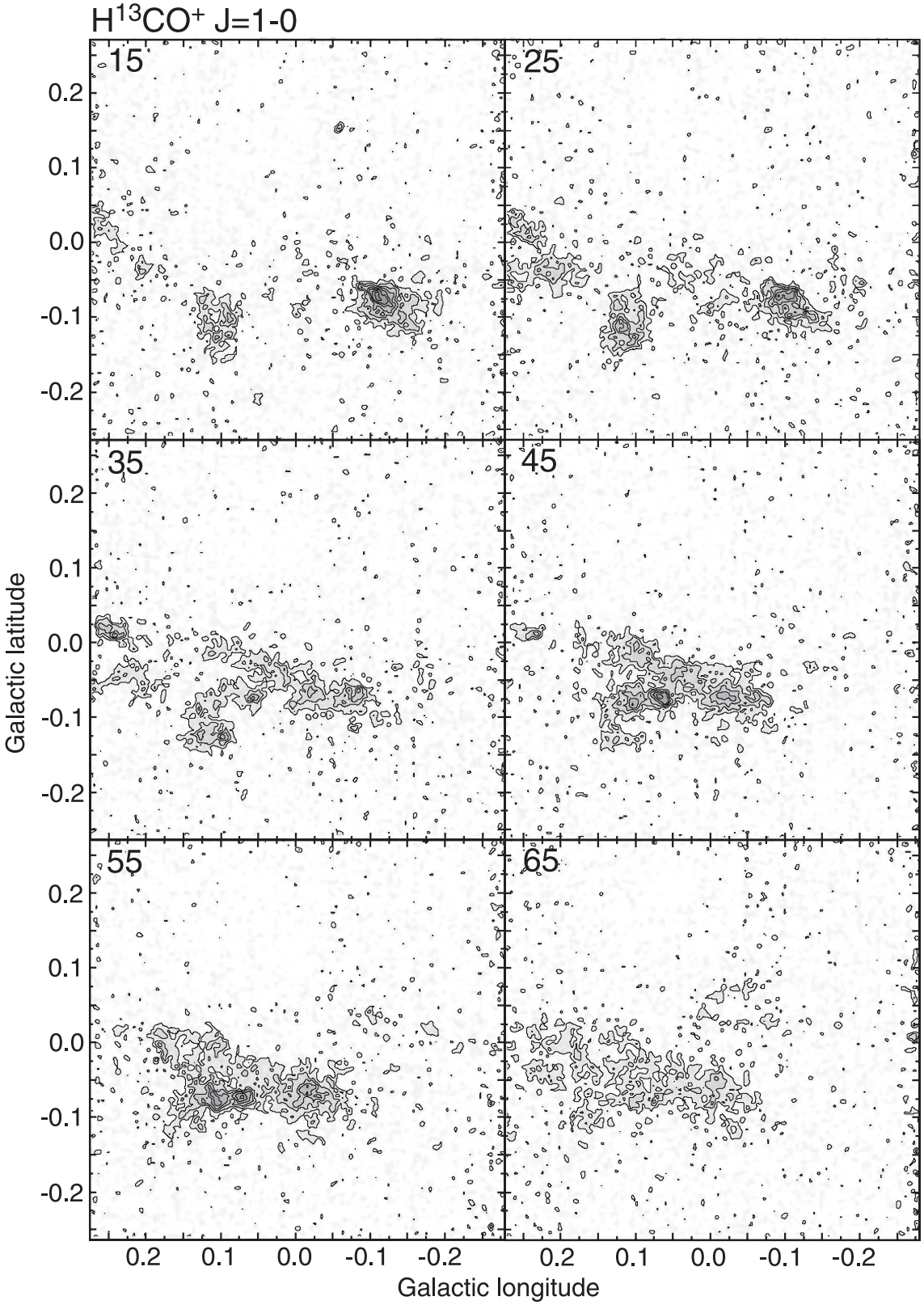

Fig. 4. (Continued)

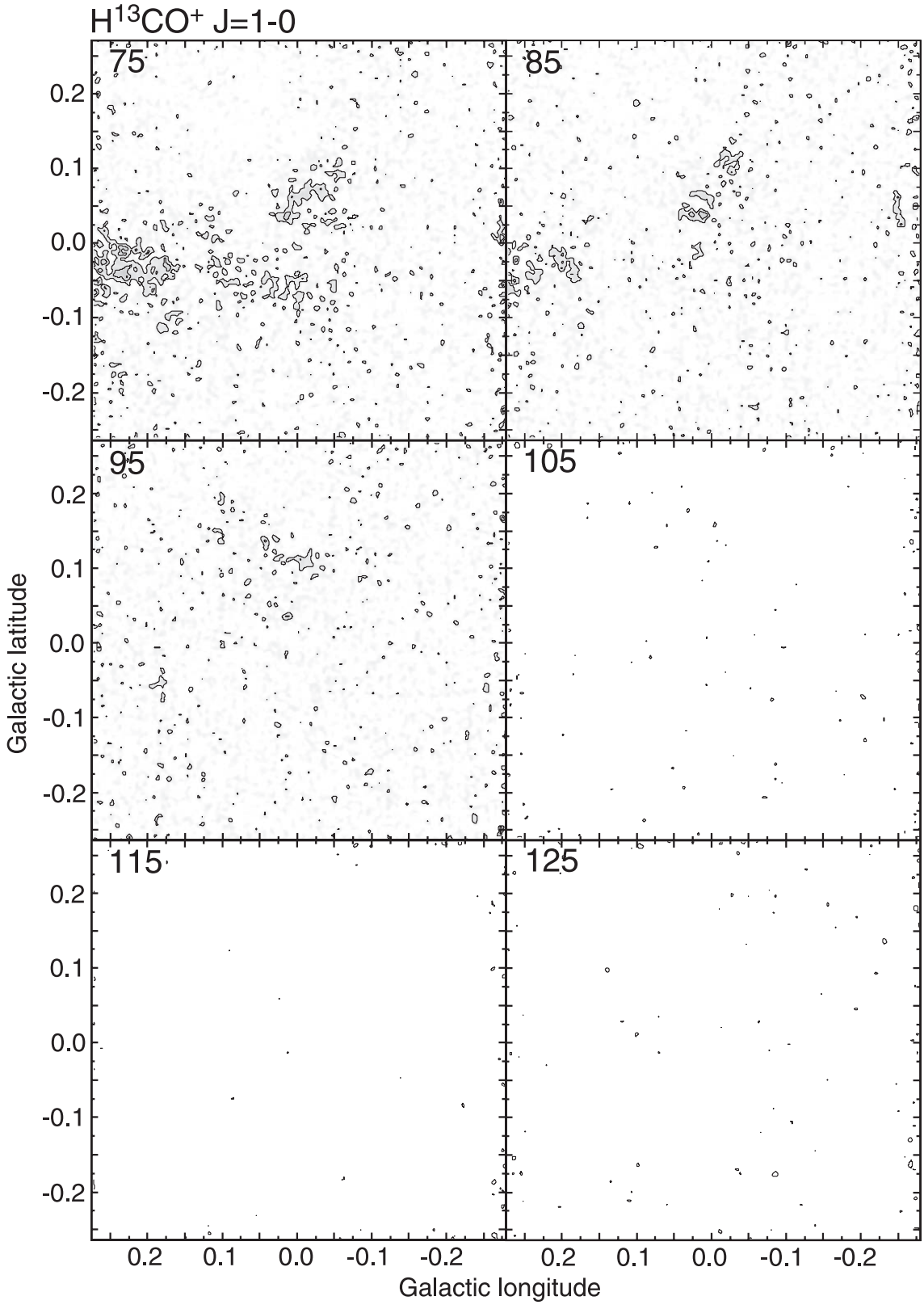

Fig. 4. (Continued)

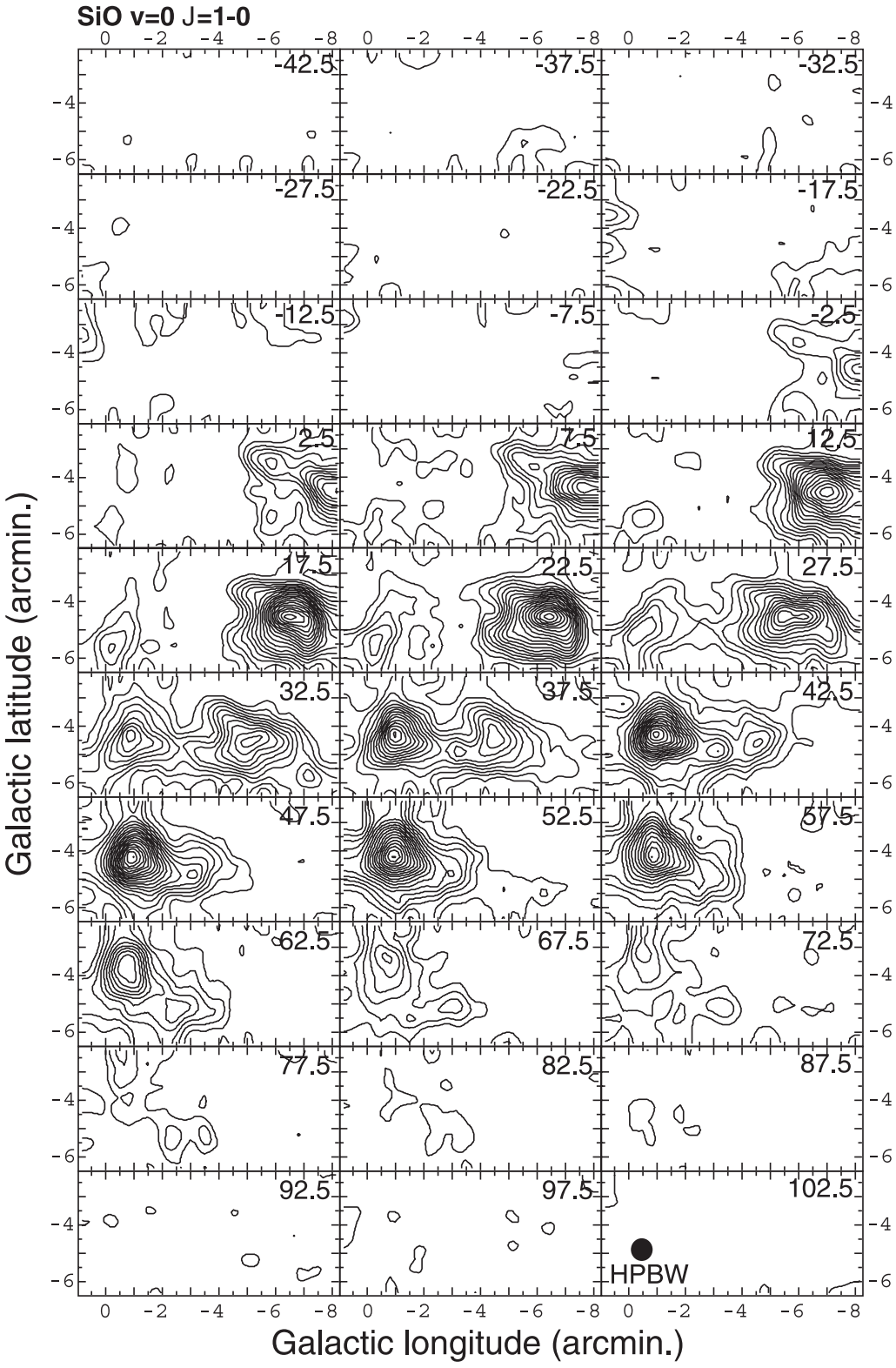

Fig. 5. Channel maps of SiO $v = 0$, $J = 1$–0 emission in the Sgr A region. The data were numerically convolved with a 30″ circular Gaussian beam. The velocity integrated width is 5 km s^{-1}. Center velocities are shown in the upper-right corner of each map. The first contour and the interval are both $T_{\rm MB} = 0.143$ K. The typical achieved r.m.s. noise in the map is 0.069 K in $T_{\rm MB}$.

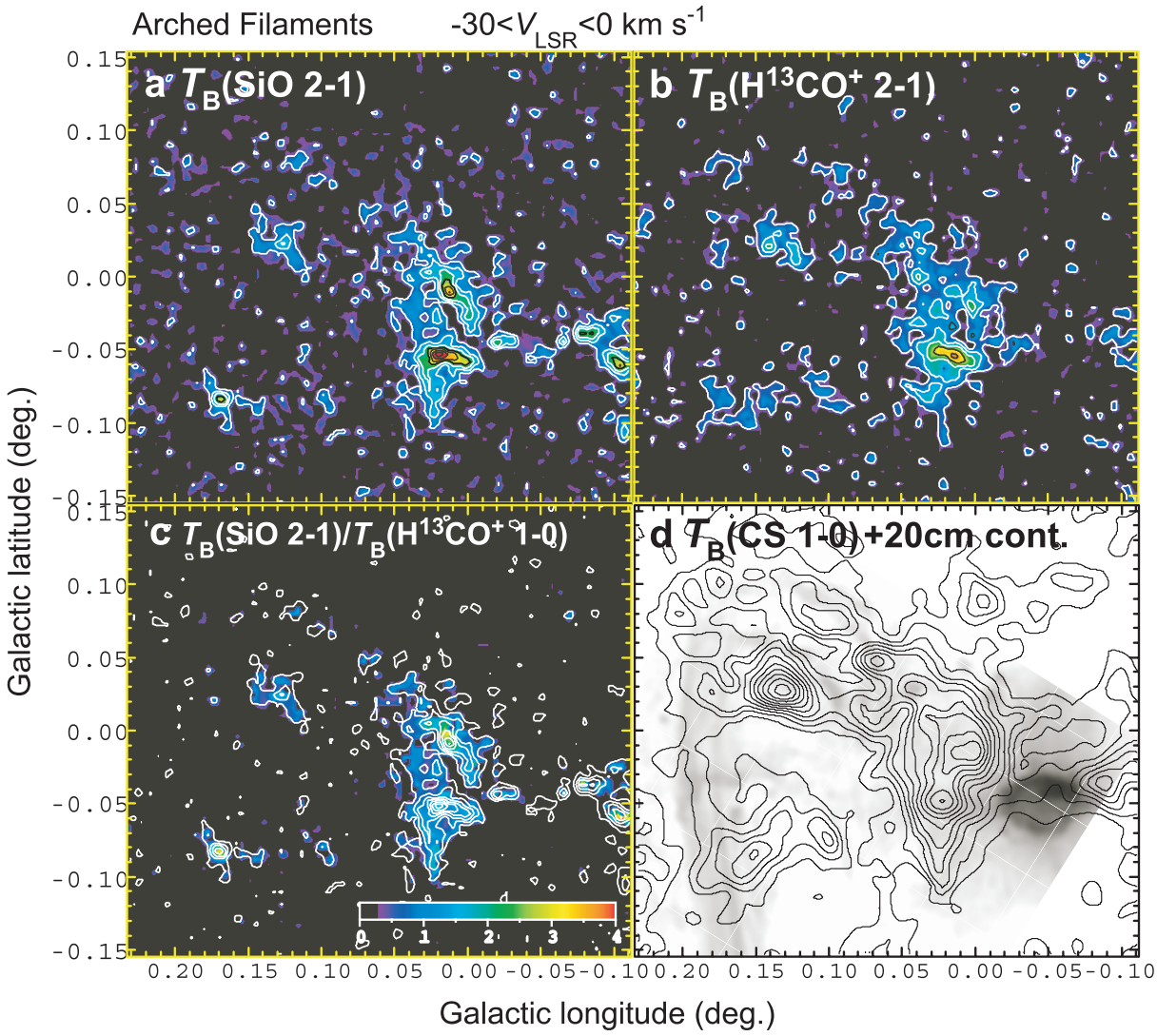

Fig. 6. (a) Velocity-integrated map (contours and pseudo color) of the molecular cloud adjoining Arched filaments in the SiO $v = 0$, $J = 2$–1 emission line. The velocity range is $V_{\rm LSR} = -30$–$0\,{\rm km\,s^{-1}}$. The contour intervals are $T_{\rm MB} = 0.102$ K. The effective beam size is FWHM $= 26''$. (b) Velocity-integrated map (contours and pseudo color) of the molecular cloud in the $H^{13}CO^+$ emission line. The velocity range is $V_{\rm LSR} = -30$–$0\,{\rm km\,s^{-1}}$. The first contour and contour interval are both $T_{\rm MB} = 0.102$ K. The effective beam size is FWHM $= 26''$. (c) Intensity ratio of the SiO and $H^{13}CO^+$ lines, $T_{\rm B}[{\rm SiO}(2\text{–}1)]/T_{\rm B}[H^{13}CO^+(1\text{–}0)]$. The contours are the same as those shown in (a). (d) Velocity-integrated map (contours) of the molecular cloud in the CS $J = 1$–0 emission line. The effective beam size is FWHM $= 60''$. Gray-scale shows the high-resolution continuum at 20 cm observed by VLA (Yusef-Zadeh & Morris 1987).

unity, $R_{\rm SiO/H^{13}CO^+} \lesssim 1$. Although the strange morphology has suggested that the Arched filaments molecular cloud was formed by events originating from shocked molecular gas, such as tidal disrupting (Serabyn & Güsten 1987) or successive supernova remnants (SNRs), the observed low brightness temperature ratio shows that there is no evidence for the production of shocked molecular gas in the molecular cloud.

3.2. *GCM 0.11−0.11 Molecular Cloud and Sickle Molecular Cloud*

The GCM 0.11−0.11 molecular cloud is located just on the negative longitude side of Vertical filaments (see figure 7d). It is widely accepted that the GCM 0.11−0.11 molecular cloud is as close as to Vertical filaments as the projection. The morphologies of GCM 0.11−0.11 in the CS and CO lines are similar (Tsuboi et al. 1997; Oka et al. 1998). The peculiar morphology and the wide velocity width of the GCM 0.11−0.11 molecular cloud suggest that the molecular cloud physically interacts with Vertical filaments (Tsuboi et al. 1997). GCM 0.11−0.11 is bright at the X-ray fluorescent iron, 6.4 keV line (e.g., Yusef-Zadeh et al. 2002). The GCM 0.11−0.11 molecular cloud is detected in the NH_3 (4, 4) emission line and higher, although the energy level of the (4, 4) excitation state reaches at least 202 K (Miyazaki et al. 2008).

The molecular cloud is clearly seen in channel maps of the SiO $v = 0$, $J = 2$–1 and $H^{13}CO^+$ $J = 1$–0 emission lines from $V_{\rm LSR} = 5\,{\rm km\,s^{-1}}$ to $V_{\rm LSR} = 55\,{\rm km\,s^{-1}}$ (see figure 3 and figure 4). Figures 7a and 7b show velocity-integrated maps of the GCM 0.11−0.11 molecular cloud in the SiO $v = 0$, $J = 2$–1 and $H^{13}CO^+$ $J = 1$–0 emission lines, respectively.

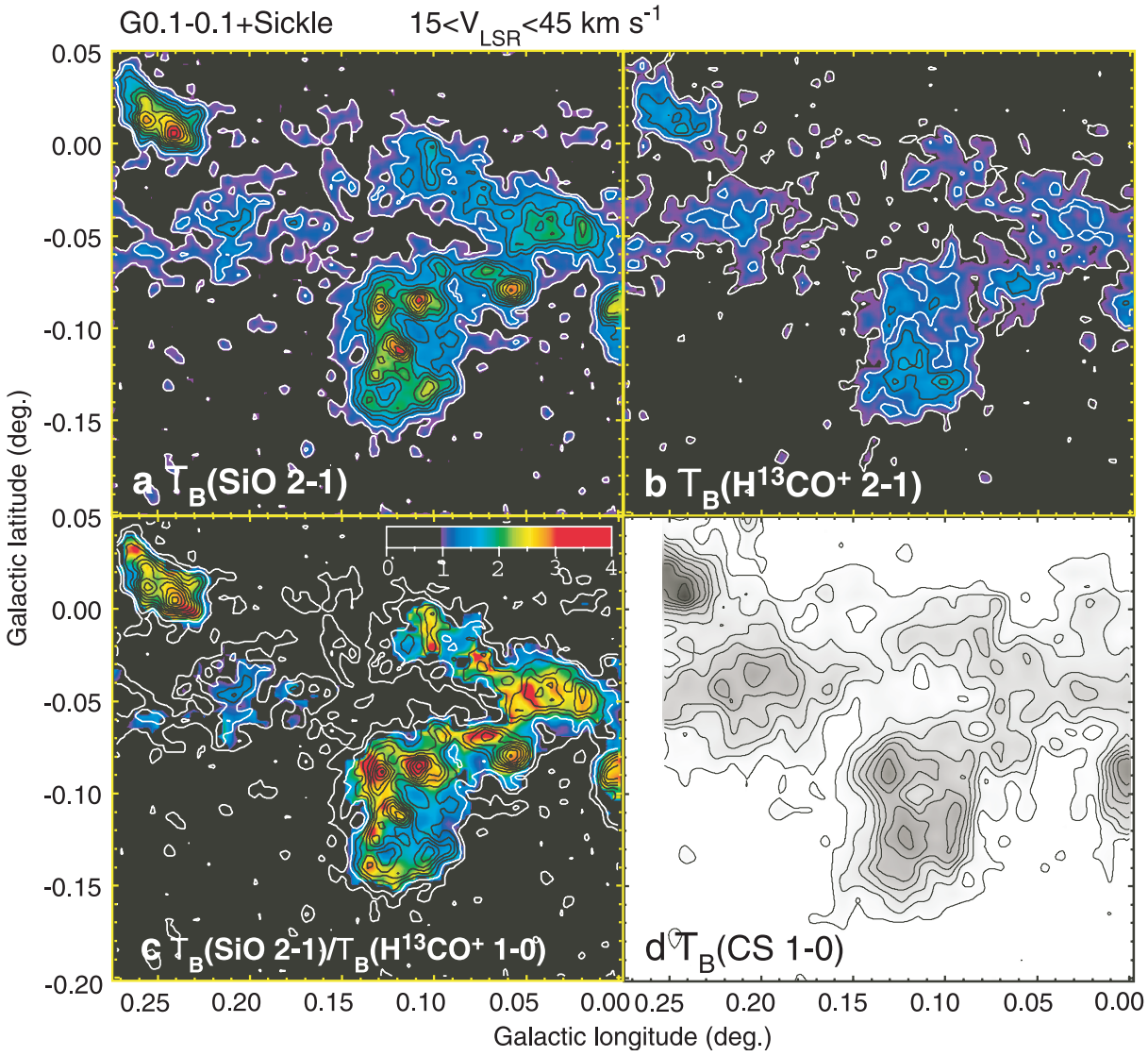

Fig. 7. (a) Velocity-integrated map in the SiO $v = 0$, $J = 2$–1 emission line of the molecular cloud adjoining Vertical filaments. The velocity range is $V_{\rm LSR} = 15$–45 km s^{-1}. The effective beam size is FWHM $= 26''$. The first contour and contour interval are both $T_{\rm MB} = 0.114$ K. (b) Velocity-integrated map of the molecular cloud in the $H^{13}CO^+$ emission line. The velocity range is $V_{\rm LSR} = 15$–45 km s^{-1}. The effective beam size is FWHM $= 26''$. The first contour and contour interval are both $T_{\rm MB} = 0.114$ K. (c) The intensity ratio of the SiO and $H^{13}CO^+$ lines, $T_{\rm B}$[SiO(2–1)]/ $T_{\rm B}$[$H^{13}CO^+$(1–0)]. (d) Velocity-integrated map of the molecular cloud in the CS $J = 1$–0 emission line. The effective beam size is FWHM $= 60''$.

The integrated velocity range is $V_{\rm LSR} = 15$–45 km s^{-1}. The molecular cloud is roughly similar in both emission lines. However, several strong intensity peaks in the cloud are seen only in the SiO emission line. The molecular cloud in the $H^{13}CO^+$ line has a more smoothed appearance. Figure 7c shows the brightness temperature ratio of the SiO and $H^{13}CO^+$ lines, $R_{\rm SiO/H^{13}CO^+}$, in this velocity range. Figure 7d shows the GCM 0.11−0.11 molecular cloud in the CS $J = 1$–0 emission line for a comparison. There is a ridge feature with a high ratio, $R_{\rm SiO/H^{13}CO^+} \simeq 4$, along the positive longitude edge of the GCM 0.11−0.11 molecular cloud. The highest ratio on the ridge corresponds to the intensity peaks of the SiO emission line. The brightness temperature ratio on the other side is approximately unity, $R_{\rm SiO/H^{13}CO^+} \simeq 1$. The distribution of the brightness temperature ratio in the cloud was not clear in the previous observation because of a sparse observation grid and insufficient signal-to-noise ratio (Handa et al. 2006). Using our higher resolution and high sensitivity image, we show that the positive longitude side of the cloud has a high ratio. The negative and positive longitude sides of GCM 0.11−0.11 have different excitation states, although both sides have similar turbulent velocities in the SiO, CS, and CO emission lines.

Sickle is a peculiar shape H II region located at $l = 0.^\circ16$, $b = -0.^\circ04$, like a bridge over Vertical filaments (Yusef-Zadeh & Morris 1987). A molecular cloud, that is associated with Sickle is remarkable in channel maps of the SiO $v = 0$, $J = 2$–1 and $H^{13}CO^+$ $J = 1$–0 emission lines from $V_{\rm LSR} = 15$ km s^{-1} to $V_{\rm LSR} = 35$ km s^{-1} (hereafter Sickle molecular cloud). The Sickle molecular cloud is clearly seen in the CS line as a more extended molecular cloud (see figure 7d).

The Sickle H II region traces the negative latitude edge of the cloud. The ridge-like emission in the SiO and $H^{13}CO^+$ lines also traces the edge (see figures 7a and 7b). The brightness temperature ratio of the ridge is up to two, $R_{\mathrm{SiO/H^{13}CO^+}} \lesssim 2$. The intensity ratio in the other portion is approximately lower than unity, $R_{\mathrm{SiO/H^{13}CO^+}} \lesssim 1$. The peculiar morphology of the Sickle molecular cloud suggests that the cloud is close to Vertical filaments, and physically interacts with them. If so, the observed low brightness temperature ratio indicates no large amount of shocked molecular gas in the cloud. Another molecular cloud positionally corresponding to Sickle is visible in both emission lines at $V_{\mathrm{LSR}} = 75$ and $85\,\mathrm{km\,s^{-1}}$ (see figure 3). However, this cloud has no detailed morphological comparison for Sickle. The physical relation between the cloud is not likely to be associated with Sickle.

The GCM 0.25+0.01 molecular cloud is located on the positive longitude side of Vertical filaments. The molecular cloud is clearly seen in both lines (also see figures 7a and 7b). No remarkable continuum source is associated with the molecular cloud. It is clearly seen in the CS line (see figure 7d), and identified as a dark cloud in near-infrared maps (Stolovy et al. 2006). The cloud has a large velocity width of up to $50\,\mathrm{km\,s^{-1}}$ in the SiO emission line (see figure 3). The cloud in the SiO line is much brighter than that in the $H^{13}CO^+$ line. The brightness temperature ratio of the cloud is larger than three, $R_{\mathrm{SiO/H^{13}CO^+}} \gtrsim 3$. This value is probably consistent with the large internal velocity width of the cloud. The GCM 0.07−0.07 molecular cloud and the GCM 0.10−0.08 molecular cloud are clearly seen in channel maps of $V_{\mathrm{LSR}} = 30$ and $70\,\mathrm{km\,s^{-1}}$ in both emission lines (also see figure 3 and figure 4).

3.3. *The 50-km s^{-1} Molecular Cloud and the 20-km s^{-1} Molecular Cloud*

Previous molecular line observations show that the $50\text{-km\,s}^{-1}$ molecular cloud (GCM −0.02−0.07) and the $20\text{-km\,s}^{-1}$ molecular cloud (GCM −0.13−0.08) are most remarkable and the densest molecular clouds in the Sgr A molecular cloud complex (e.g., Oka et al. 1998; Tsuboi et al. 1999). The $20\text{-km\,s}^{-1}$ molecular cloud appears to be connected to the $50\text{-km\,s}^{-1}$ molecular cloud by an extended molecular bridge.

Figure 8 shows channel maps of the molecular clouds around Sgr A, of which the left and right sides are those in the SiO $v = 0$, $J = 2$–1 and $H^{13}CO^+$ $J = 1$–0 emission lines, respectively. These are enlarged maps of figures 3 and 4. The $50\text{-km\,s}^{-1}$ molecular cloud in the SiO $v = 0$, $J = 1$–0 emission line has a triangular shape. Such appearance is also seen in the integrated intensity map of the CS $J = 1$–0 emission line (Tsuboi et al. 1999). Although the $50\text{-km\,s}^{-1}$ molecular cloud is detected with a high signal-to-noise ratio in the channel maps from $V_{\mathrm{LSR}} = 7.5\,\mathrm{km\,s^{-1}}$ to $V_{\mathrm{LSR}} = 72.5\,\mathrm{km\,s^{-1}}$ in the SiO emission lines, the cloud is significantly weaker in the channel maps of the $H^{13}CO^+$ emission line. Meanwhile, the $20\text{-km\,s}^{-1}$ molecular cloud is detected with a high signal-to-noise ratio in the channel maps from $V_{\mathrm{LSR}} = 7.5\,\mathrm{km\,s^{-1}}$ to $V_{\mathrm{LSR}} = 72.5\,\mathrm{km\,s^{-1}}$ in both emission lines. The interior structures of the $50\text{-km\,s}^{-1}$ molecular cloud are clearly seen in the channel maps of the SiO $v = 0$, $J = 2$–1 and $H^{13}CO^+$ $J = 1$–0 emission lines. As pointed out with the previous Nobeyama Millimeter Array (NMA) observation in the CS emission line (Tsuboi et al. 2009), the interior structures of the $50\text{-km\,s}^{-1}$ molecular cloud is made of several compact components and an extended component connecting them. Three distinct components identified with NMA are also identified as strong components in the SiO line. Compact components with $V_{\mathrm{LSR}} = 10$–$30\,\mathrm{km\,s^{-1}}$ are alined toward the Galactic center, itself. Meanwhile, these components are identified only as weak features in the $H^{13}CO^+$ emission line. The $H^{13}CO^+$ emission line also presents a clumpy distribution of the molecular cloud.

Figure 9 shows the brightness temperature ratio (pseudo color) of the SiO and $H^{13}CO^+$ emission lines, $R_{\mathrm{SiO/H^{13}CO^+}}$, overlaid on the integrated intensity map of the SiO emission line (contours). The component centered at $l = 0\overset{\circ}{.}001$ and $b = -0\overset{\circ}{.}092$ is visible in the velocity range from 5 to $40\,\mathrm{km\,s^{-1}}$ (see figure 8). This component is identified as two neighboring compact components in NMA higher resolution maps in the CS $J = 1$–0 line (see figure 2 in Tsuboi et al. 2009). This disappears in the $H^{13}CO^+$ emission line. The second component is centered at $l = -0\overset{\circ}{.}015$ and $b = -0\overset{\circ}{.}082$ from 15 to $45\,\mathrm{km\,s^{-1}}$ in the SiO line. This is much weaker in the $H^{13}CO^+$ emission line. These are identified as high brightness temperature ratio areas in figures 9b and 9c. The highest ratio is as high as eight, $R_{\mathrm{SiO/H^{13}CO^+}} \simeq 8$. These are presumably made of shocked molecular gas. There is third component centered at $l = -0\overset{\circ}{.}020$ and $b = -0\overset{\circ}{.}070$ from 20 to $75\,\mathrm{km\,s^{-1}}$ in the SiO line. The extension from the $20\text{-km\,s}^{-1}$ molecular cloud along the Sgr A East shell blends in the third component. This component is weak, but identified in the $H^{13}CO^+$ emission line. This is also identified as a high brightness temperature ratio area in figures 9b and 9c. In the velocity range from 50 to $75\,\mathrm{km\,s^{-1}}$, another component is north of the third component. The center of this component is moving to north with an increase of the velocity. The forth component is not identified in the $H^{13}CO^+$ emission line. They are remarkable only in the SiO emission line. The brightness temperature ratio of the structures is as high as $R_{\mathrm{SiO/H^{13}CO^+}} = 2$–8. They are presumably shock-originated features. The detailed interior structures in the cloud are discussed in the next section.

Meanwhile, the $20\text{-km\,s}^{-1}$ molecular cloud stretches roughly along a line inclined to the Galactic plane by 20°, and has a large velocity gradient along the major axis (e.g., Tsuboi et al. 1999; Oka et al. 1998). The innermost part in projection distance has been discussed as the start point of gas fueling from the molecular cloud to the Sgr A West or circum-nuclear disk (CND) (e.g., Ho et al. 1985; Okumura et al. 1989). The gas fueling from molecular clouds may play an important role in the activity of the Sgr A region. The detailed interior structures in the cloud are also discussed in the next section.

4. Discussion

4.1. *Molecular Gas Mass of the Sgr A Molecular Cloud Complex*

The molecular clouds of the Sgr A molecular cloud complex have been believed to be dense enough to be gravitationally stable against the tidal shear produced by the supermassive black hole of the Galactic center (Stark et al. 1989). As

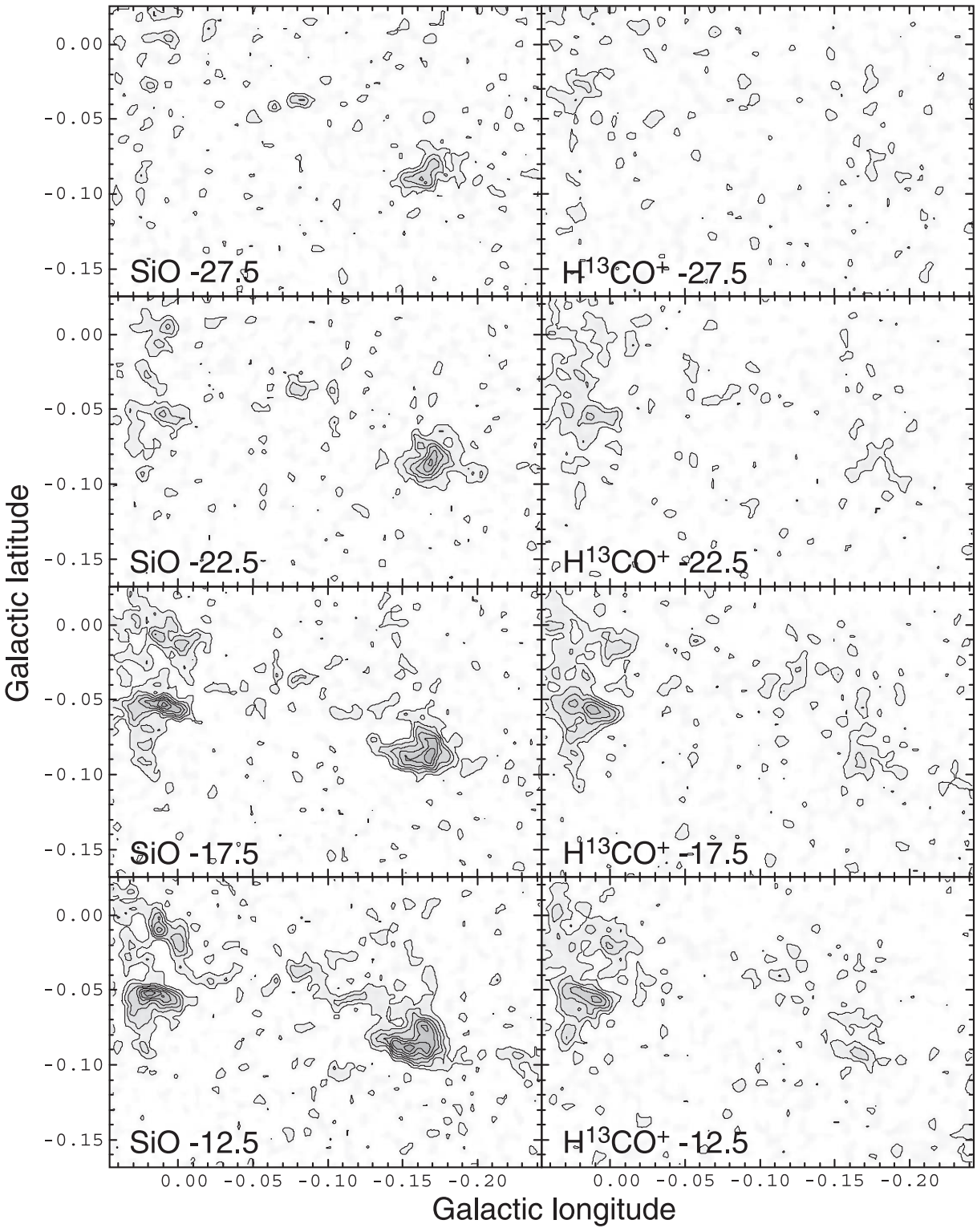

Fig. 8. Channel maps of the 50-km s^{-1} and 20-km s^{-1} molecular clouds in the SiO $v = 0$, $J = 2$–1 and $H^{13}CO^{+}$ $J = 1$–0 emission lines. The left panels are for SiO and the right panels are for $H^{13}CO^{+}$. The data were numerically convolved with a 20″ circular Gaussian beam. The velocity integrated width is 5 km s^{-1}. The emission lines and center velocities are shown in the lower-left corner of each map. The first contour and contour interval are $T_{\rm MB} = 0.182$ K. The typical achieved noise level in the map is 0.079 K in $T_{\rm MB}$.

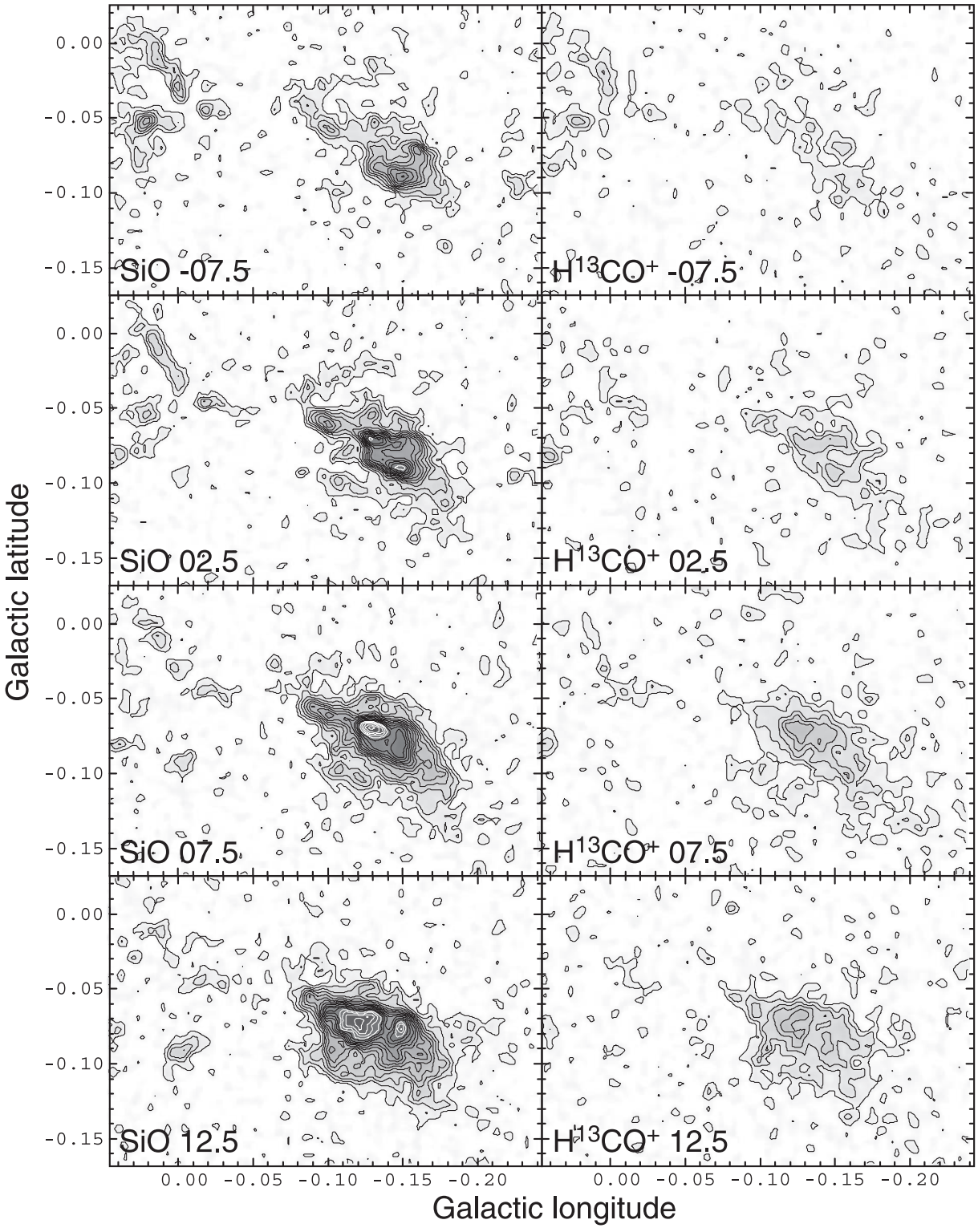

Fig. 8. (Continued)

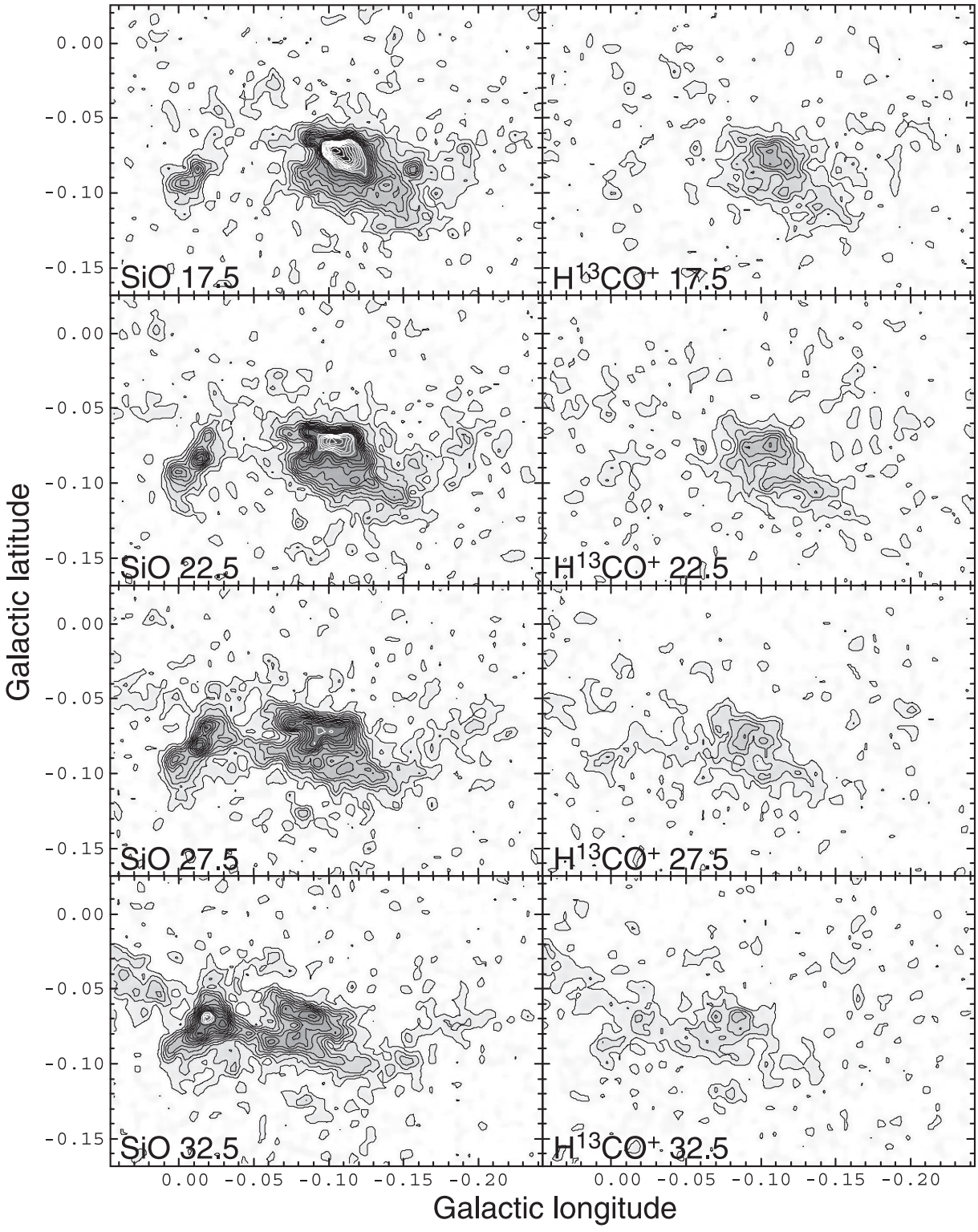

Fig. 8. (Continued)

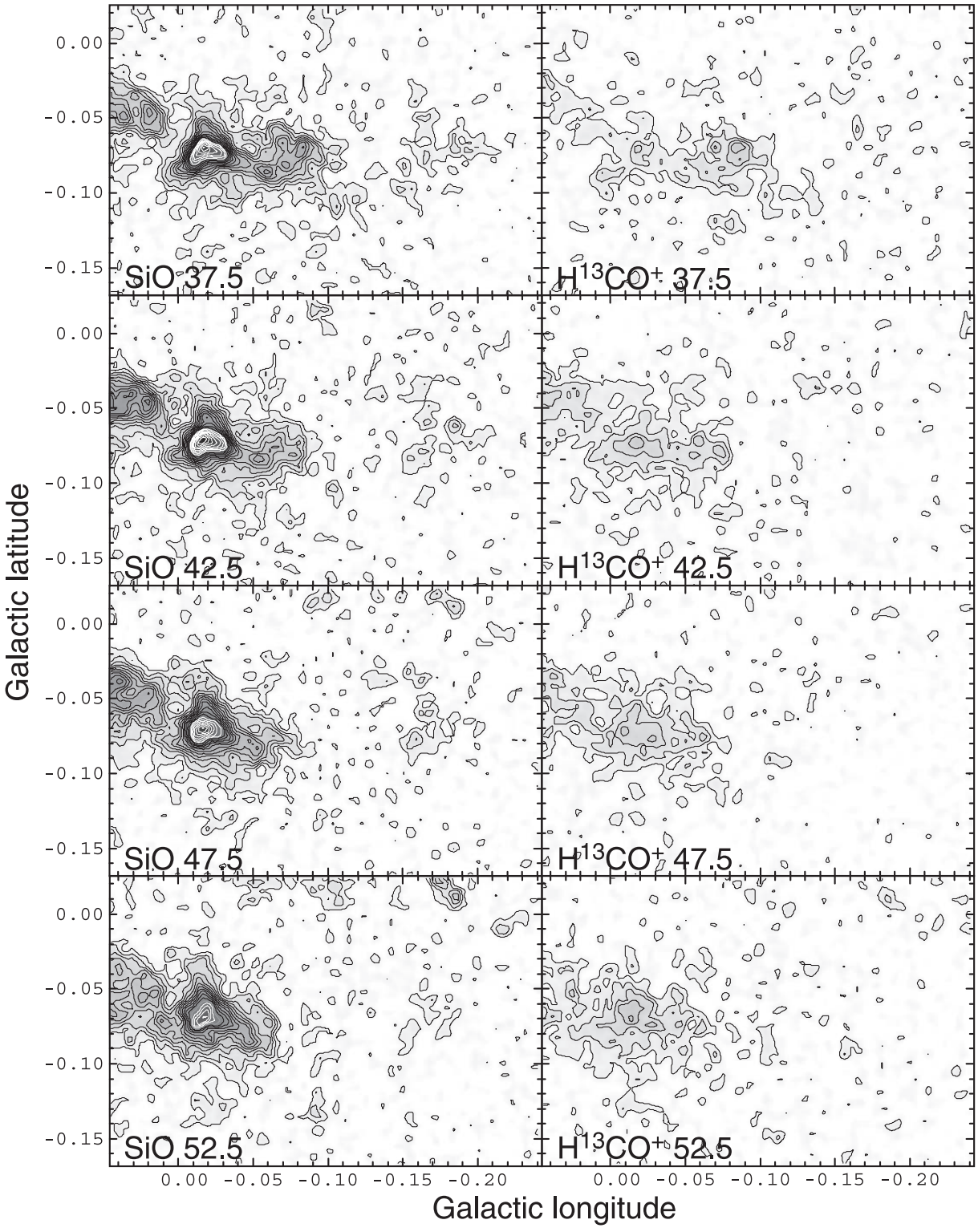

Fig. 8. (Continued)

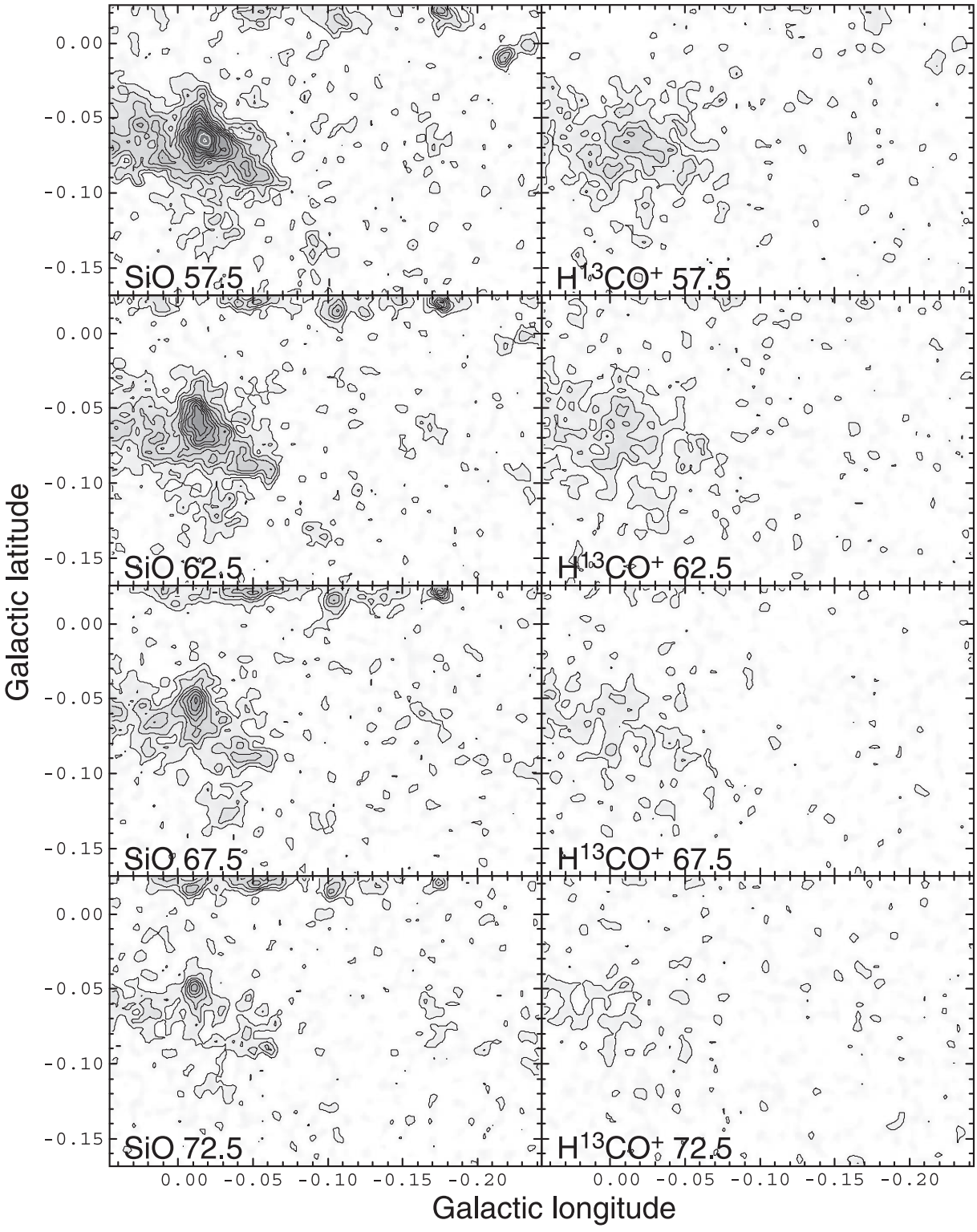

Fig. 8. (Continued)

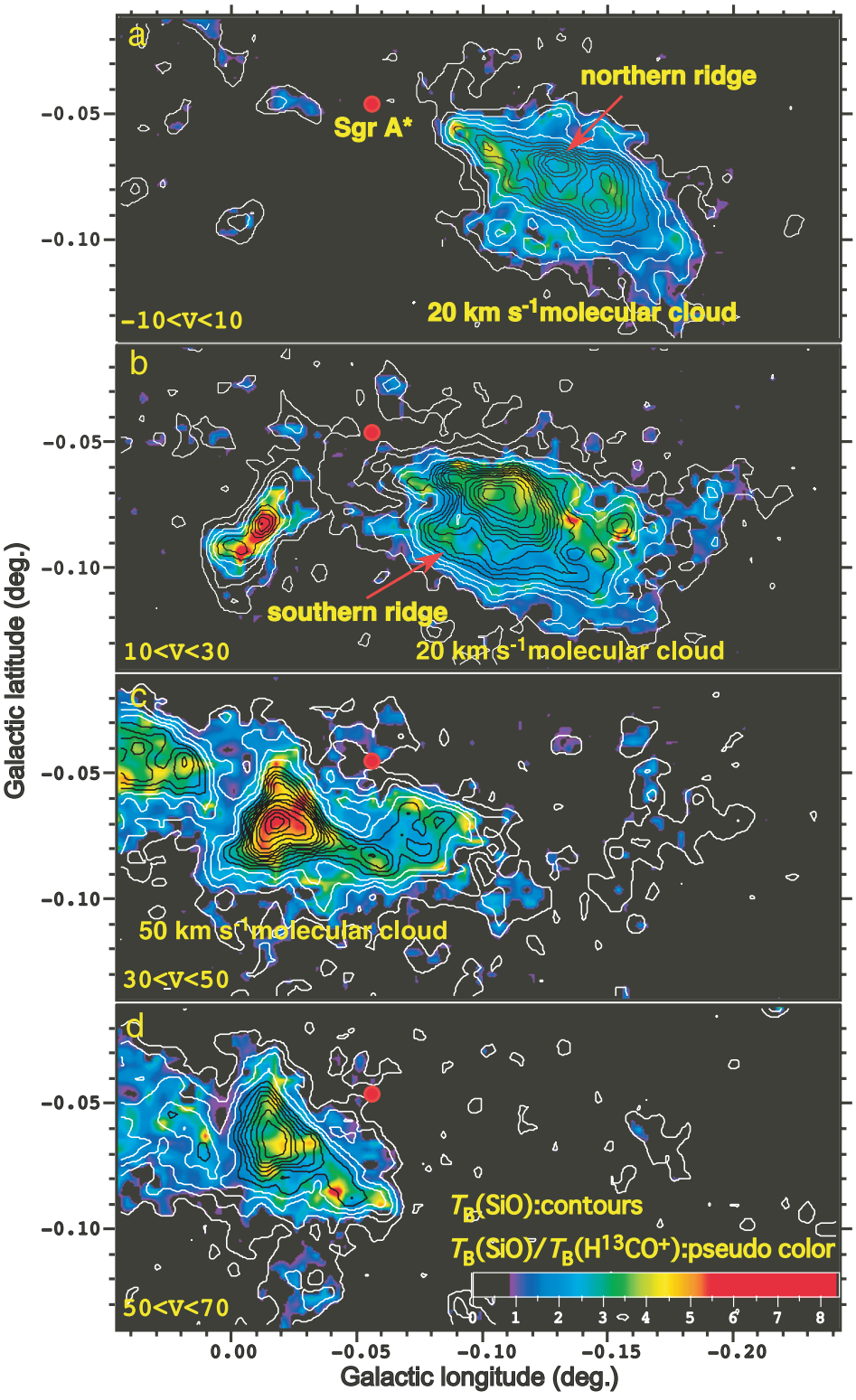

Fig. 9. Brightness temperature ratio of the SiO $v = 0$, $J = 2$–1 and $H^{13}CO^+$ $J = 1$–0 emission lines (pseudo color), $T_B(\mathrm{SiO})/T_B(H^{13}CO^+)$, overlaid on the integrated intensity map of the SiO $v = 0$, $J = 2$–1 emission line (contours). (a) $V_{LSR} = -10$–$10\,\mathrm{km\,s^{-1}}$. The red filled circle shows the position of Sgr A*. (b) $V_{LSR} = 10$–$30\,\mathrm{km\,s^{-1}}$. (c) $V_{LSR} = 30$–$50\,\mathrm{km\,s^{-1}}$. (d) $V_{LSR} = 50$–$70\,\mathrm{km\,s^{-1}}$. The contour levels are 0.227, 0.455, 0.682, 0.909, 1.136, 1.364, 1.590, 1.818, 2.045, 2.500, 2.955, and 3.409 K in T_{MB}. The color bar of brightness temperature ratio is shown on panel (d).

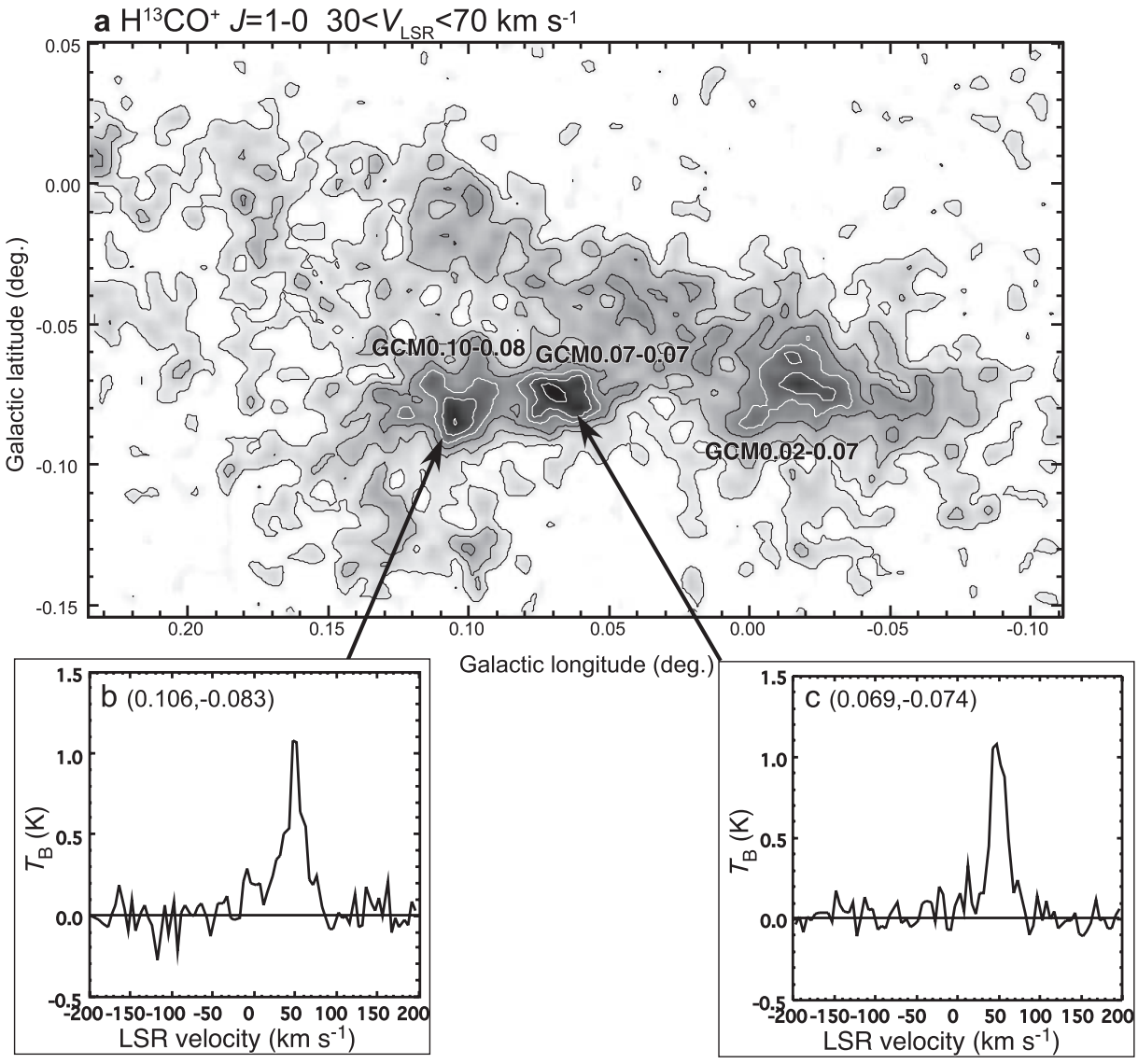

Fig. 10. (a) Velocity-integrated intensity map (contours and gray scale) of the GCM 0.07−0.07 and GCM 0.10−0.07 molecular clouds in the $H^{13}CO^+$ $J = 1$–0 emission line. The velocity-integrated range is from 30 to 50 km s^{-1}. The first contour and the interval are both $T_{\rm MB} = 0.143$ K. The typical achieved r.m.s. noise in the map is 0.102 K in $T_{\rm MB}$. (b) $H^{13}CO^+$ $J = 1$–0 emission line spectrum of the GCM 0.10−0.07 molecular cloud. (c) $H^{13}CO^+$ $J = 1$–0 emission line spectrum of the GCM 0.07−0.07 molecular cloud.

shown in figure 8 and figure 9, the $H^{13}CO^+$ $J = 1$–0 emission line in the 50-km s^{-1} molecular cloud (GCM −0.02−0.07) is several-times weaker than the SiO $v = 0$, $J = 2$–1 line, although the 20-km s^{-1} molecular cloud (GCM −0.13−0.08) in the $H^{13}CO^+$ emission line resembles that in the SiO line. The observed difference in the appearances of the 50-km s^{-1} molecular cloud suggests that SiO-enriched gas presumably occupies a large volume of the 50-km s^{-1} molecular cloud, and that the column density is not so dense as to produce a high brightness temperature of the $H^{13}CO^+$ emission line. Then, the previous image based on CS and CO observations (e.g., Oka et al. 1998; Tsuboi et al. 1999) may be required to be revised. An alternate to make the observed property is depletion of the $H^{13}CO^+$ molecule. If so, we need to explain why they have a large velocity width of over 30 km s^{-1}. These hypotheses are discussed later in this subsection.

4.1.1. *Virial theorem mass*

Virial theorem mass has been used for a mass estimation of molecular clouds, at least in the disk region of the Galaxy. In the case of optically thin in an emission line with a Gaussian profile, no external pressure, and no magnetic filed, the virial theorem mass of a spherical cloud with uniform density is nominally calculated by

$$M_{\rm vir}\ (M_\odot) = 210 \times \Delta V_{1/2}({\rm km\ s^{-1}})^2 R({\rm pc}), \qquad (1)$$

where $\Delta V_{1/2}$ is the FWHM of an emission-line profile (see Miyazaki & Tsuboi 2000). Figure 10 shows a velocity-integrated intensity map of the GCM 0.07−0.07 and GCM 0.10−0.08 molecular clouds and the spectra at the intensity peaks. The line profiles are shown by a single Gaussian function. These clouds are suitable for this analysis because they have simple and compact structures. The FWHM widths

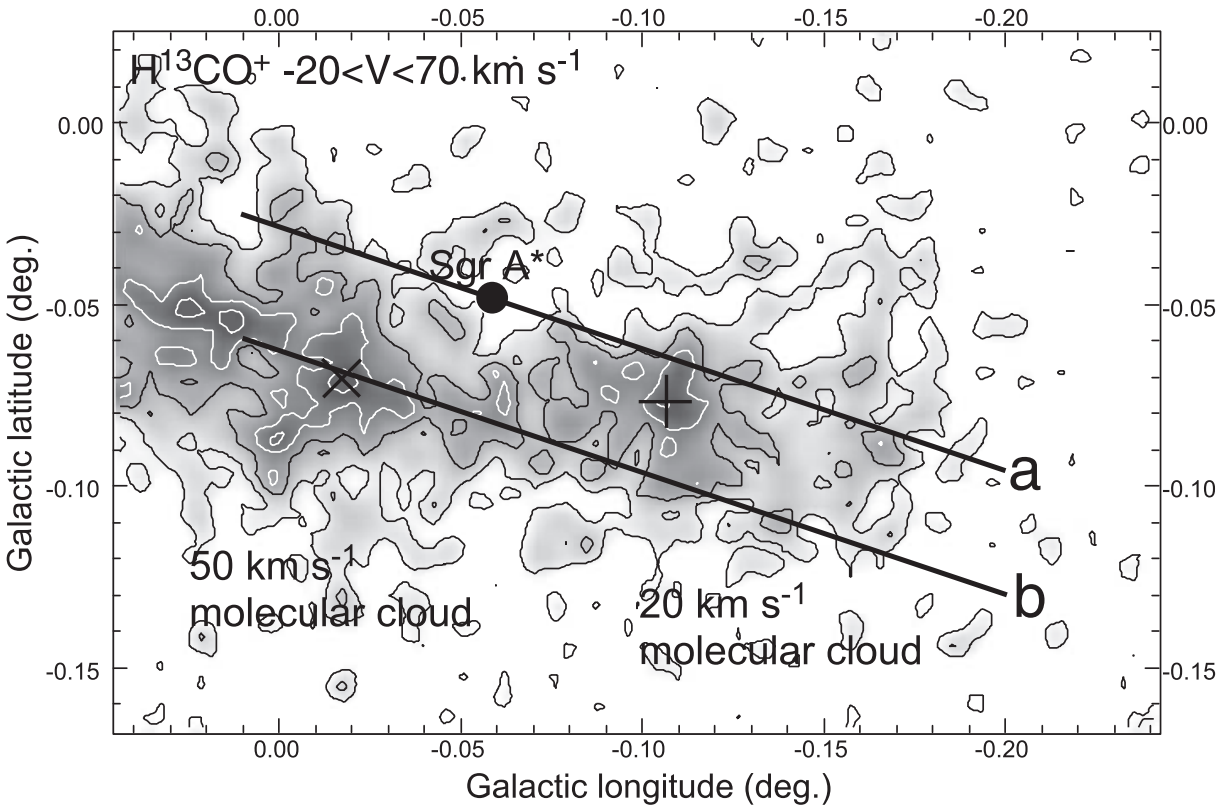

Fig. 11. Velocity-integrated intensity map (contours and gray scale) of the 50-km s^{-1} molecular cloud (GCM −0.02−0.07) and the 20-km s^{-1} molecular cloud (GCM −0.13−0.08) in the $H^{13}CO^+$ $J = 1$–0 emission line. The velocity range is $V_{\rm LSR} = -20$–70 km s^{-1}. The first contour and contour interval are both $T_{\rm MB} = 0.102$ K; the 50-km s^{-1} molecular cloud has a triangle-shape feature centered at $l = -1'02''$ ($-0\overset{\circ}{.}0173$), $b = -4'16''$ ($-0\overset{\circ}{.}0712$). The position–velocity diagrams along the thick lines, (a) and (b), are shown in figure 12. Cross and plus marks in the figure show the positions of the peak column densities of H_2 of the 50-km s^{-1} and 20-km s^{-1} molecular clouds. The values are $N_{\rm H_2} = 7.7 \times 10^{23}$ cm^{-2} at $l = -1'02''$ ($-0\overset{\circ}{.}017$), $b = -4'16''$ ($-0\overset{\circ}{.}071$) and $N_{\rm H_2} = 6.7 \times 10^{23}$ cm^{-2} at $l = -6'25''$ ($-0\overset{\circ}{.}107$), $b = -4'37''$ ($-0\overset{\circ}{.}077$), respectively.

of these molecular clouds are both about $\Delta V_{1/2} \simeq 20$ km s^{-1} in the $H^{13}CO^+$ $J = 1$–0 emission line. The virial theorem masses of the GCM 0.07−0.07 and GCM 0.10−0.08 molecular clouds are calculated to be $M_{\rm vir} \simeq 1.9 \times 10^5\, M_\odot$ and $M_{\rm vir} \simeq 1.7 \times 10^5\, M_\odot$, respectively.

Figure 11 shows a velocity-integrated intensity map of the 50-km s^{-1} molecular cloud (GCM −0.02−0.07) and the 20-km s^{-1} molecular cloud (GCM −0.13−0.08) in the $H^{13}CO^+$ $J = 1$–0 emission line. The case of the 20-km s^{-1} molecular cloud is fairly difficult because of the complexity of its kinetic structure. The 20-km s^{-1} molecular cloud consists of parallel northern and southern ridges stretching along a line inclined to the Galactic plane by 20° (see figure 10 and also see figures 9a and 9b). Some bridging structures connect these ridges. Figures 12a and 12b show position–velocity diagrams in the $H^{13}CO^+$ $J = 1$–0 emission line along the inclined lines from $l = 0\overset{\circ}{.}011$, $b = -0\overset{\circ}{.}024$ to $l = -0\overset{\circ}{.}201$, $b = -0\overset{\circ}{.}093$ (line a in figure 11) and from $l = 0\overset{\circ}{.}011$, $b = -0\overset{\circ}{.}063$ to $l = -0\overset{\circ}{.}201$, $b = -0\overset{\circ}{.}133$ (line b in figure 11). Line a is the major axis of the northern ridge. Line b is the major axis of the southern ridge, which is connected to the 50-km s^{-1} molecular cloud. The FWHM width of the 20-km s^{-1} molecular cloud is about $\Delta V_{1/2} \simeq 38$ km s^{-1}. The velocity width of the 20-km s^{-1} molecular cloud is caused not only by the internal gas motion, but also by the velocity gradient in the cloud along the Galactic longitude and blending of the both ridges. The velocity width without these external contributions is estimated to be $\Delta V_{1/2} \simeq 24$ km s^{-1} (also see figure 2). The virial theorem mass of the 20-km s^{-1} molecular cloud is probably $M_{\rm vir} \simeq 8.0 \times 10^5\, M_\odot$.

The case of the 50-km s^{-1} molecular cloud is also difficult for the same reason. The FWHM of the $H^{13}CO^+$ line profile integrated in the 50-km s^{-1} molecular cloud is nominally $\Delta V_{1/2} \simeq 40$ km s^{-1}. The virial theorem mass of the 50-km s^{-1} molecular cloud is estimated to be $M_{\rm vir} \leq 1 \times 10^6\, M_\odot$. There are physical interactions with SNRs in the cloud. Such interactions presumably produce unbounded gas with a large velocity width. In addition, there are several sub-structures in the cloud. These will be discussed in the later subsection. These presumably lead to an overestimation of the virial theorem mass. The masses of the named molecular clouds in the Sgr A complex are given in table 1.

4.1.2. LTE molecular gas mass

We also estimated the molecular gas mass from $H^{13}CO^+$ $J = 1$–0 integrated intensity (see figure 4 and figure 8) under the condition of local thermal equilibrium (LTE) and an optically thin limit. The column density of H_2 based on $H^{13}CO^+$ $J = 1$–0 observations is given by

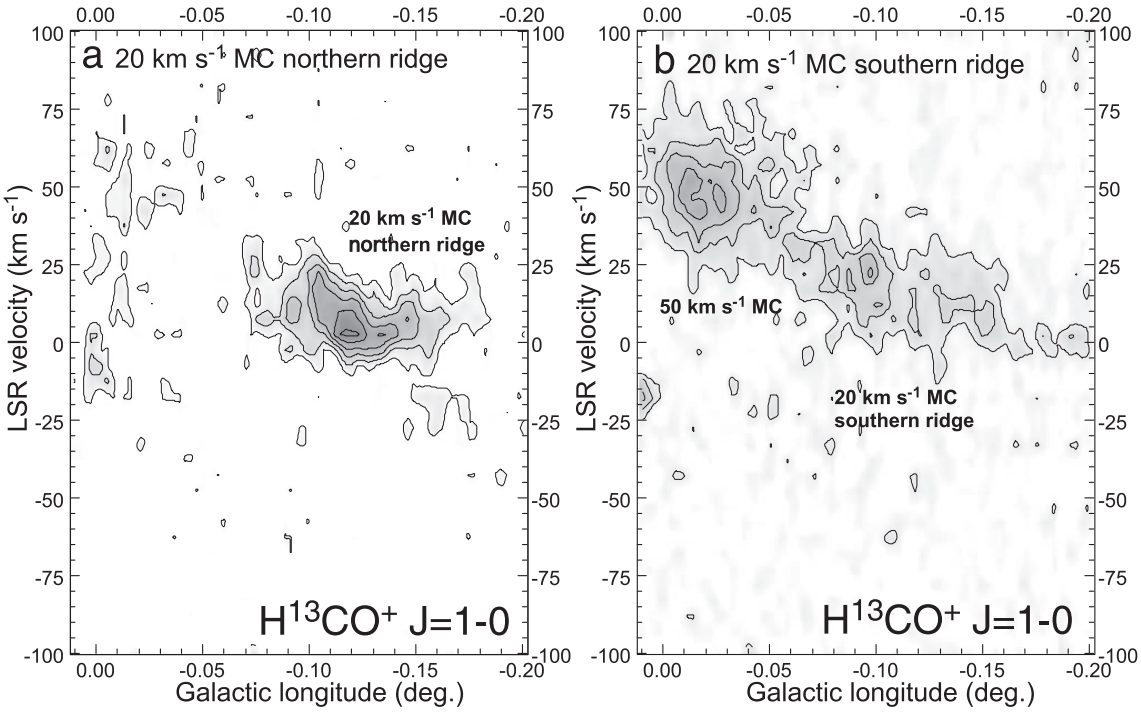

Fig. 12. Position–velocity diagrams of the 20-km s^{-1} molecular cloud (GCM −0.13−0.08) in the $H^{13}CO^+$ $J = 1$–0 emission line along the lines (a) and (b) in figure 11. (a) From $l = 0.^\circ011$, $b = -0.^\circ024$ to $l = -0.^\circ201$, $b = -0.^\circ093$, which is the major axis of the northern ridge of the 20-km s^{-1} molecular cloud. The position offset of $0.^\circ01$ corresponds to about 1 pc in these diagrams. The first contour and contour interval are both 0.2 K in $T_{\rm MB}$. (b) From $l = 0.^\circ011$, $b = -0.^\circ063$ to $l = -0.^\circ201$, $b = -0.^\circ133$, which is the major axis of the southern ridge. The first contour and contour interval are both 0.2 K in $T_{\rm MB}$.

Table 1. Mass of the molecular clouds in the Sgr A molecular cloud complex.

Molecular cloud	$M_{\rm LTE}$* ($M_\odot$)	$M_{\rm vir}$ ($M_\odot$)	$M_{350\mu{\rm m}}$†,‡ ($M_\odot$)	$M_{800\mu{\rm m}}$†,§ ($M_\odot$)	$M_{850\mu{\rm m}}$†,‖ ($M_\odot$)
GCM −0.13−0.08	2.3×10^5	8.0×10^5	4.8×10^5	5.0×10^5	7.8×10^5
GCM −0.02−0.07	1.1×10^5	$\leq 1 \times 10^6$	2.4×10^5	4.0×10^5	5.0×10^5
GCM 0.07−0.07	1.9×10^5	1.8×10^5			
GCM 0.10−0.08	1.7×10^5	1.7×10^5			
GCM 0.11−0.11	1.0×10^5		3.9×10^5		3.8×10^5
Arch	7.5×10^5				
Sickle	0.6×10^5				
GCM 0.25+0.01	2.0×10^5				3.5×10^5

* We assumed $X(H^{13}CO^+) = (1.8 \pm 0.4) \times 10^{-11}$ and $T_{\rm ex} = 7$ K.
† We assumed $T_{\rm dust} = 20$ K and $Z/Z_\odot = 2$.
‡ Dowell et al. (1999).
§ Lis and Carlstrom (1994).
‖ Pierce-Price et al. (2000).

$$N_{\rm H_2}\,({\rm cm}^{-2}) = \frac{5.99 \times 10^{10} T_{\rm ex} \int T_{\rm MB} dv ({\rm K\ km\ s}^{-1})}{X(H^{13}CO^+)}. \quad (2)$$

Here, $T_{\rm ex}$ and $X(H^{13}CO^+)$ are the excitation temperature and the fractional abundance, $X(H^{13}CO^+) = N(H^{13}CO^+)/N_{\rm H_2}$, of an $H^{13}CO^+$ molecule. We calculated the molecular mass of the cloud from the derived distribution of the H_2 column density. The molecular mass is given by

$$M_{\rm LTE}\,(M_\odot) = \Omega({\rm cm}^2)\mu(M_\odot) \sum_m \sum_n N_{\rm H_2}(m,n)({\rm cm}^{-2}), \quad (3)$$

where Ω is the physical area corresponding to the sampling grid, $\Omega = 7.89 \times 10^{35}$ cm^2 for a 7″ grid spacing at the Galactic center distance and μ is the mean mass per one H_2 molecule, $\mu = 1.94 \times 10^{-57}\,M_\odot$.

Table 2. Peak column density of the molecular clouds in the Sgr A molecular cloud complex.

Molecular cloud	l (°)	b (°)	Peak integrated intensity $\int T_{\rm MB} dv$ (K km s^{-1})	Peak column density* $N_{\rm H_2}$ (cm^{-2})
GCM −0.13−0.08	−0.107	−0.077	29.0	6.7×10^{23}
GCM −0.02−0.07	−0.017	−0.071	33.1	7.7×10^{23}
GCM 0.07−0.07	0.069	−0.074	26.1	6.1×10^{23}
GCM 0.10−0.08	0.106	−0.083	24.8	5.8×10^{23}
GCM 0.11−0.11	0.103	−0.130	21.6	5.0×10^{23}
Arch	0.013	−0.054	16.4	3.8×10^{23}
Sickle	0.212	−0.041	9.7	2.3×10^{23}
GCM 0.25+0.01	0.242	0.007	19.4	4.5×10^{23}

* We assumed $X(\rm H^{13}CO^+) = 1.8 \times 10^{-11}$ and $T_{\rm ex} = 7$ K.

In this case, there are two factors with large umbiguity: the excitation temperature and the fractional abundance of the $\rm H^{13}CO^+$ molecule. The $\rm NH_3$ observation indicates that the rotational temperatures of the 50-km s^{-1} and 20-km s^{-1} molecular clouds are $T_{\rm rot} = 80$ K and 60 K, respectively (Miyazaki et al. 2008). It has been conventionally assumed that the excitation temperature of a relatively abundant molecule, like CS, is $T_{\rm ex} = 50$–60 K, because the excitation temperature is usually lower than the rotational temperature derived from $\rm NH_3$ observations (e.g., Tsuboi et al. 1999). However, recent LVG analyses for several emission lines of less-abundant molecules, including SiO and $\rm H^{13}CO^+$, show that the molecules are clearly in sub-thermal in the Galactic center region (Amo-Baladrón et al. 2009). Our analysis using the SiO $J = 1$–0 and $J = 2$–1 emission lines is shown in a later section. From analysis, we here assume that the excitation temperature of the $\rm H^{13}CO^+$ molecule is $T_{\rm ex} = 7$ K. The LTE molecular masses of the GCM 0.07−0.07 molecular cloud and the GCM 0.10−0.08 molecular cloud, are $M_{\rm LTE} = 3.53 \times 10^{-6}/X(\rm H^{13}CO^+)\ M_\odot$ and $M_{\rm LTE} = 3.08 \times 10^{-6}/X(\rm H^{13}CO^+)\ M_\odot$, respectively. From a comparison between the virial theorem masses and the LTE masses, the fractional abundance of $\rm H^{13}CO^+$ of GCM 0.07−0.07 and GCM 0.10−0.08 are estimated to be $X(\rm H^{13}CO^+) = 1.8 \times 10^{-11}$ and $X(\rm H^{13}CO^+) = 1.8 \times 10^{-11}$, respectively. The average value is $X(\rm H^{13}CO^+) = (1.8 \pm 0.4) \times 10^{-11}$. This is one third of the value accepted for the Orion Giant Molecular Cloud, $X(\rm H^{13}CO^+) = 5 \times 10^{-11}$ (Ikeda et al. 2007).

We would estimate the LTE molecular line mass of other named molecular clouds of the Sgr A molecular cloud complex. The LTE molecular line masses of the 50-km s^{-1} and 20-km s^{-1} molecular clouds were calculated to be $M_{\rm LTE} = 1.1 \times 10^5\ M_\odot$ and $M_{\rm LTE} = 2.3 \times 10^5\ M_\odot$, respectively. The LTE molecular mass of the GCM 0.11−0.11 molecular cloud is $M_{\rm LTE} = 1.0 \times 10^5\ M_\odot$. The LTE mass based on the previous $\rm H^{13}CO^+$ observation is $M_{\rm LTE} = 4.51 \times 10^5\ M_\odot$ (Handa et al. 2006). The LTE molecular masses of the Arched filaments molecular cloud and the GCM 0.25+0.01 molecular cloud are $M_{\rm LTE} = 7.5 \times 10^5\ M_\odot$ and $2.0 \times 10^5\ M_\odot$, respectively. The LTE masses of the named molecular clouds in the Sgr A complex are also given in table 1. As mentioned in the previous subsection, the fractional abundance of $\rm H^{13}CO^+$ is estimated to be $X(\rm H^{13}CO^+) = (1.8 \pm 0.4) \times 10^{-11}$ in these molecular clouds.

The column densities of the named molecular clouds in the Sgr A complex are given in table 2. The peak column densities of $\rm H_2$ of the 50-km s^{-1} molecular cloud is $N_{\rm H_2} = 7.7 \times 10^{23}$ cm^{-2} at $l = -6'25''$ ($-0\overset{\circ}{.}107$), $b = -4'37''$ ($-0\overset{\circ}{.}077$), respectively (see figure 2 and figure 11). This value is twice larger than the observed value at the molecular cloud, GCM 0.11−0.11, which was the largest known of any, even in the Galactic center region at the present, $N_{\rm H_2} = 4 \times 10^{23}$ cm^{-2} (Handa et al. 2006). The source size of the 50-km s^{-1} molecular cloud on the celestial sphere is estimated to be 6 pc (also see figure 8 and figure 11), or $D = 2 \times 10^{19}$ cm. We assume that the line-of-sight length is equal to the source physical size on the celestial sphere. Then, the average $\rm H_2$ density in the cloud is derived to be $\bar{n}_{\rm H_2} \simeq N_{\rm H_2}/D = 4 \times 10^4$ cm^{-3} around the intensity peak. The derived column density of the 50-km s^{-1} molecular cloud converts to visual extinction, $A_V = N_{\rm H_2}({\rm cm^{-2}})/[1.9 \times 10^{21}\ ({\rm cm^{-2}\,mag^{-1}})] = 400$ mag or K-band extinction, $A_K = 0.15 A_V = 60$ mag. The K-band extinction is consistent with the appearance in Spitzer maps (Stolovy et al. 2006) as the "IR dark cloud".

On the other hand, the molecular mass of the molecular cloud was also estimated with the column density of a hydrogen atom converted from thermal dust emission. The masses of the named molecular clouds in the Sgr A complex are also given in table 1. The molecular mass of the 50-km s^{-1} molecular cloud based on 350 μm (Dowell et al. 1999), 800 μm (Lis & Carlstrom 1994), and 850 μm (Pierce-Price et al. 2000) observations are $M_{350\mu\rm m} = 2.4 \times 10^5\ M_\odot$, $M_{800\mu\rm m} = 4.0 \times 10^5\ M_\odot$, and $M_{850\mu\rm m} = 5.0 \times 10^5\ M_\odot$, assuming that the dust temperature is $T_{\rm dust} = 20$ K. The average value is $M_{\rm ave} = (3.8 \pm 1.3) \times 10^5\ M_\odot$. A comparison between the mass and the LTE mass based on the $\rm H^{13}CO^+$ observation provides another estimate of the fractional abundance of $\rm H^{13}CO^+$. The value is estimated to be $X(\rm H^{13}CO^+) = (5 \pm 2) \times 10^{-12}$. While the molecular masses of the 20-km s^{-1} molecular cloud are $M_{350\mu\rm m} = 4.8 \times 10^5\ M_\odot$ for the 350 μm observation, $M_{800\mu\rm m} = 5 \times 10^5\ M_\odot$ for the 800 μm observation, and $M_{850\mu\rm m} = 7.8 \times 10^5\ M_\odot$ for the 850 μm observation. The average value is $M_{\rm ave} = (5.9 \pm 1.7) \times 10^5\ M_\odot$. Using the same procedure as mentioned above, the fractional abundance is estimated to be $X(\rm H^{13}CO^+) = (7 \pm 2) \times 10^{-12}$. The fractional abundance of these named clouds may be lower than the

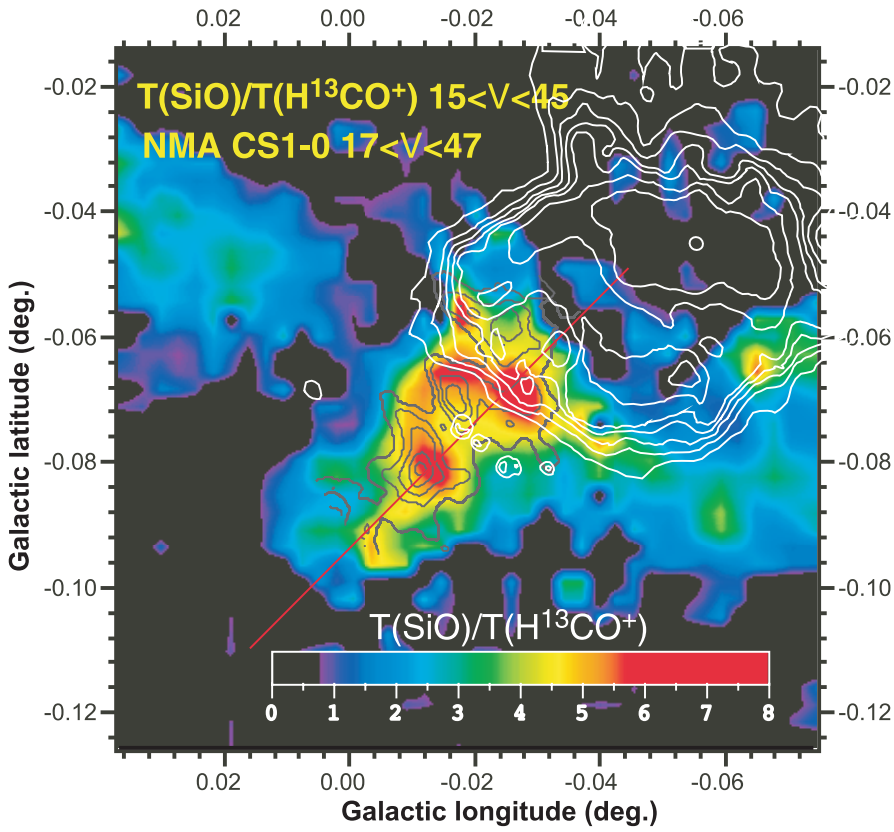

Fig. 13. Brightness temperature ratio of the SiO $v = 0$, $J = 2$–1, and $H^{13}CO^+$ $J = 1$–0 emission lines (pseudo color), $R_{\mathrm{SiO/H^{13}CO^+}} = T_{\mathrm{B}}(\mathrm{SiO})/T_{\mathrm{B}}(\mathrm{H^{13}CO^+})$, of the 50-km s^{-1} molecular cloud (GCM −0.02−0.07). The velocity integrated range is $V_{\mathrm{LSR}} = 15$–45 km s^{-1}. There is a shell-like feature in the cloud. The black contours show a CS $J = 1$–0 velocity integrated map observed by NMA (Tsuboi et al. 2009). The white contours show an image of Sgr A at 5 GHz observed by VLA (Yusef-Zadeh & Morris 1987). The position–velocity diagram along the red line is shown in figure 14.

fractional abundance from the comparison between the virial theorem masses and the LTE masses based on the observation of GCM 0.07−0.07 and GCM 0.10−0.08. The depletion of $H^{13}CO^+$ molecules presumably explains the weakness of the $H^{13}CO^+$ emission line in the 50-km s^{-1} molecular cloud. The depletion is not consistent with that the isotope ratio of C in the Galactic center region decreases to $^{12}C/^{13}C \sim 17$, or one third of the value in the Galactic disk (Milam et al. 2005), which usually leads to an increase in the fractional abundance of the $H^{13}CO^+$ molecule. In addition, the UV flux and the free electron density in the Galactic center may affect the fractional abundance.

4.2. *Shocked Molecular Gas in the Sgr A Molecular Cloud Complex*

4.2.1. *Expanding molecular shell in the 50-km s^{-1} molecular cloud*

The 50-km s^{-1} molecular cloud (GCM −0.02−0.07) is presumably interacting with the Sgr A East (e.g., Ho et al. 1985; Yusef-Zadeh et al. 2001), which is an SNR shell located behind the Sgr A West (Pedlar et al. 1989). Our NMA observation indicates that the shocked contact surface exists in the molecular cloud (Tsuboi et al. 2009). In addition it also suggests the presence of an expanding shell-like structure in the molecular cloud. This shell-like structure may correspond to a "hole" of the [C II] line in the molecular cloud (see figure 2 in Poglitsch et al. 1991).

Figure 13 shows the brightness temperature ratio, $R_{\mathrm{SiO/H^{13}CO^+}}$ (pseudo color), in the 50-km s^{-1} molecular cloud, and also shows the continuum emission at 5 GHz observed with VLA (white contours; Yusef-Zadeh & Morris 1987), which indicates the positional relation between the interior structures of the molecular cloud and the Sgr A East shell. The half circle-like feature with a high ratio of $R_{\mathrm{SiO/H^{13}CO^+}} \sim 4$–8 is clearly identified in the 50-km s^{-1} molecular cloud. The remarkable feature is centered at $l = -0.^\circ017$, $b = -0.^\circ074$. The diameter of the feature is about $\theta \simeq 60''$, or $D \simeq 2.5$ pc. The figure also shows the integrated intensity observed with NMA in the CS $J = 1$–0 line (black contours; Tsuboi et al. 2009). This half circle-like feature is also identified as a chain of compact components in the NMA map. This is an SiO-enriched ring-like structure that is apart from the Sgr A East shell, although the northwest edge contacts slightly with the shell.

Figure 14a shows a position–velocity diagram of the 50-km s^{-1} molecular cloud in the SiO $v = 0$, $J = 2$–1 emission

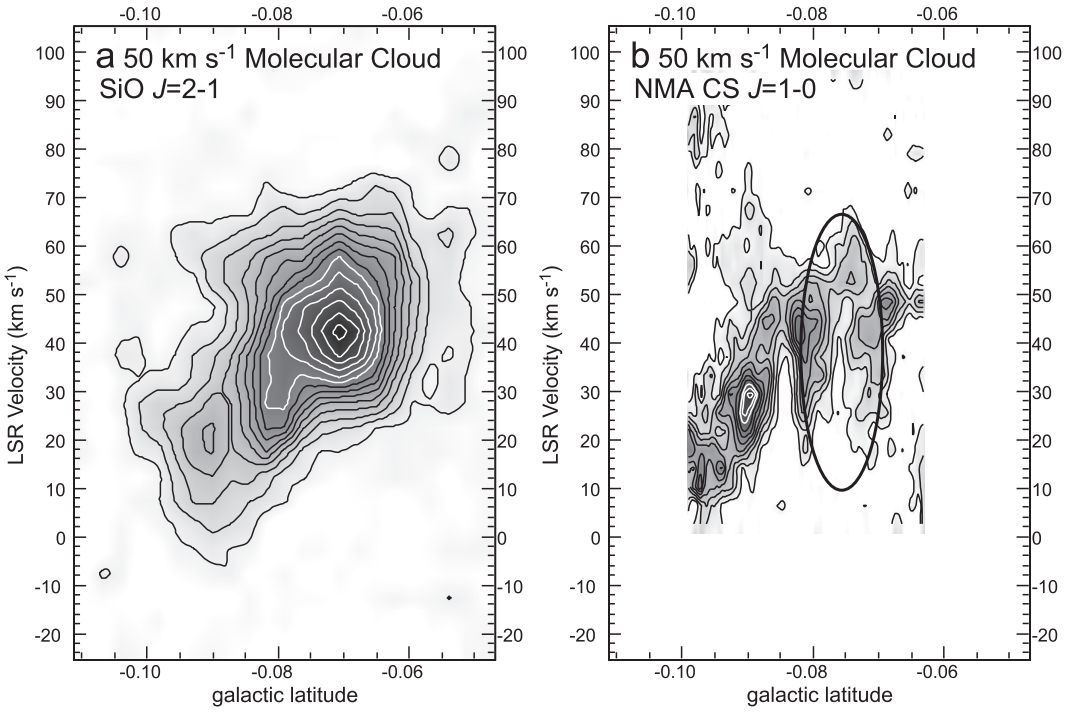

Fig. 14. (a) Position–velocity diagram of the 50-km s^{-1} molecular cloud (GCM −0.02–0.07) in the SiO $v = 0$, $J = 2$–1 emission line along the red line in figure 13. The first contour and contour interval are both 0.227 K in $T_{\rm MB}$. (b) Position–velocity diagram of the 50-km s^{-1} molecular cloud in CS $J = 1$–0 emission using NMA for a comparison. An oval indicates an expanding shell feature shown in figure 13.

line along the red line in figure 13. The velocity width of the shell is $\Delta V = 50\,{\rm km\,s^{-1}}$ at the maximum. Figure 14b shows a position–velocity diagram of the 50-km s^{-1} molecular cloud in the CS $J = 1$–0 emission line using NMA for a comparison. A higher resolution CS map indicates the expanding molecular shell as being an oval feature, although other features are also seen. The expanding velocity is estimated to be as large as 25 km s^{-1}. The diameter of the oval is $D \simeq 2.5$ pc, which is the same as the value derived from figure 13. The thickness of the shell is $t \simeq 0.3$ pc. The structure is not thought to be made by an interaction with the Sgr A East shell. Meanwhile, our 43-GHz and 94-GHz continuum observation with the NRO 45-m telescope found a continuum emission centered at the cloud (Tsuboi et al. 2009). Because the continuum component has a steep spectrum, it is presumably an SNR. The structure is thought to be an expanding molecular shell dominated by shocked molecular gas in the 50-km s^{-1} molecular cloud. The expanding molecular shell is presumably driven by the embedding SNR.

This feature is not identified in the channel maps of the $H^{13}CO^+$ line, although it is seen as a faint oval feature in the position–velocity diagram (see figure 12b). It is thus difficult to estimate the H_2 density. Here we use a critical density of the CS $J = 1$–0 emission line: $n_{\rm H_2} = 1 \times 10^4\,{\rm cm^{-3}}$. The kinetic energy of the expanding molecular shell is estimated to be 2×10^{49} erg. This energy is less than the maximum kinetic energy provided by a single supernova. Also, if the expanding velocity is constant during expansion, the age of the shell is estimated to be 4×10^4 yr. This should be the upper limit of the age.

Figure 13 also shows that a curved ridge with a high temperature ratio is surrounding the southeast boundary of the Sgr A East shell. The curved ridge is just inside the southeast boundary of the Sgr A East shell. The brightness temperature ratio of the ridge is in the range of $R_{\rm SiO/H^{13}CO^+} = 3$–6. This ratio is consistent with those of shocked gas in the 50-km s^{-1} molecular cloud and the Sgr B2 cloud (Tsuboi et al. 2011). The suggestive morphology and the high ratio suggest the physical interaction between it and the shell. In addition, a protruding component from the 50-km s^{-1} molecular cloud makes a dent, or a break, in the Sgr A East shell around $l = -0\overset{\circ}{.}03$, $b = -0\overset{\circ}{.}06$ (also see figure 13). The 36 GHz Class I methanol maser is detected in the component (Sjouwerman et al. 2010). Some parts of the curved ridge are also identified in the H_2 emission line, which are activated by shock (Yusef-Zadeh et al. 2001). These facts suggest that the surrounding component is presumably caused by the Sgr A East shell.

4.2.2. *Shocked molecular gas in the 20-km s^{-1} molecular cloud*

As mentioned previously, the 20-km s^{-1} molecular cloud (GCM −0.13−0.08) consists of parallel northern and southern ridges stretching along a line inclined to the Galactic plane by 20°. Figures 15a and 15b show position–velocity diagrams in the SiO emission line along the inclined lines from $l = 0\overset{\circ}{.}011$, $b = -0\overset{\circ}{.}024$ to $l = -0\overset{\circ}{.}201$, $b = -0\overset{\circ}{.}093$ and from $l = 0\overset{\circ}{.}011$, $b = -0\overset{\circ}{.}063$ to $l = -0\overset{\circ}{.}201$, $b = -0\overset{\circ}{.}133$ (see figure 11). The structure connecting these ridges is also seen from $l = -0\overset{\circ}{.}076$, $b = -0\overset{\circ}{.}088$ to $l = -0\overset{\circ}{.}076$, $b = -0\overset{\circ}{.}066$ in the SiO channel maps in the velocity range of $V_{\rm LSR} = 15$–35 km s^{-1}, and such structure is not clear in the $H^{13}CO^+$ channel maps (see

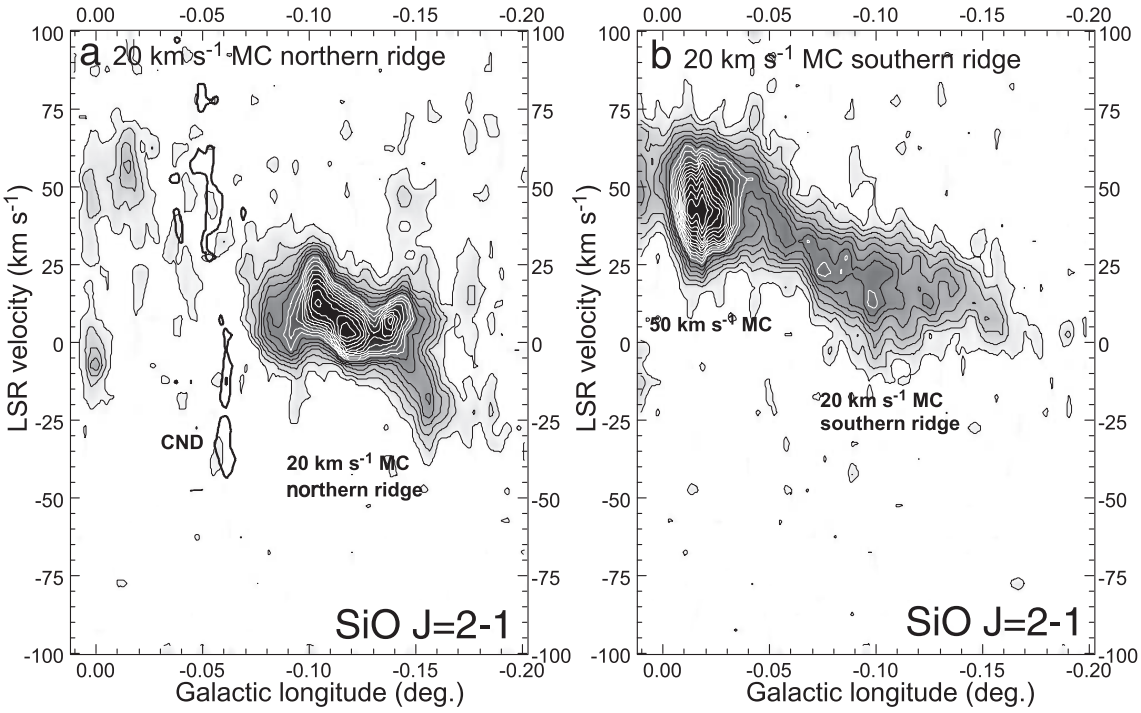

Fig. 15. (a) Position–velocity diagram of the 20-km s^{-1} molecular cloud (GCM −0.13−0.08) in the SiO $v = 0$, $J = 2$–1 emission line along the northern ridge from $l = 0\overset{\circ}{.}011$, $b = -0\overset{\circ}{.}024$ to $l = -0\overset{\circ}{.}201$, $b = -0\overset{\circ}{.}093$ [see figure 9a and also see line (a) in figure 11]. The first contour and contour interval are both 0.227 K in $T_{\rm MB}$. Thick contours show the components that belong to CND. These are located 20″ north of the major axis of the northern ridge. (b) Position–velocity diagram along the southern ridge from $l = 0\overset{\circ}{.}011$, $b = -0\overset{\circ}{.}063$ to $l = -0\overset{\circ}{.}201$, $b = -0\overset{\circ}{.}133$ [see figure 9b and also see line (b) in figure 11]. The first contour and contour interval are both 0.227 K in $T_{\rm MB}$.

figure 8). There is a clear difference between the appearances of the northern ridge in the $H^{13}CO^+$ $J = 1$–0 and SiO $v = 0$, $J = 2$–1 emission lines. The SiO emission line is much stronger than the $H^{13}CO^+$ emission line. The brightness temperature ratio is higher than $R_{\rm SiO/H^{13}CO^+} \gtrsim 3$ (see figure 12b). The northern ridge in the SiO emission line has a large velocity gradient along the major axis up to $dV/dr \simeq 4.7$ (km s^{-1} pc^{-1}). On the other hand, the extension with negative longitude and large negative velocity are not identified in the position–velocity diagram in the $H^{13}CO^+$ emission line along the northern ridge (see figure 12a). The northern ridge in the $H^{13}CO^+$ emission line has a smaller velocity gradient up to $dV/dr \simeq 2$ (km s^{-1} pc^{-1}). The eastern end of the northern ridge, the innermost part in projection distance, presumably reaches to the southern limb of the central molecular ring, CND (also see figure 9b). An inflection point of the northern ridge is located at around $l = -0\overset{\circ}{.}1$ in figure 15a. The component inner to this point has a velocity gradient with opposite sign. Figure 15a also shows that the components belong to CND (thick contours). These components are located 20″ north of the major axis of the northern ridge. The innermost part of the northern ridge seems to point toward the negative velocity end of CND. Such a velocity gradient of the northern ridge may imply a connection between the innermost part and CND. An NMA observation shows a large velocity width of the component around the contact point, although it is weak (Sato & Tsuboi 2008). This part is also remarkable in the SiO channel maps of 32.5 and 37.5 km s^{-1} in figure 8. The corresponding component has a higher temperature ratio. The brightness temperature ratio is higher than $R_{\rm SiO/H^{13}CO^+} \gtrsim 4$. This also suggests that the eastern end of the northern ridge is as close as to the Galactic center as the projection on the celestial sphere. In addition, the 36 GHz Class I methanol maser is detected around the eastern end (Sjouwerman et al. 2010). The eastern end of the northern ridge may be responsible for gas fueling from the innermost part to CND.

Meanwhile, the southern ridge extends to at least the 50-km s^{-1} molecular cloud, and bridges both molecular clouds (see figures 9a, 9b, and 9c). The appearance of the southern ridge of the 20-km s^{-1} molecular cloud in the SiO line resembles that in the $H^{13}CO^+$ line in the velocity range of $V_{\rm LSR} = 0$–50 km s^{-1}. This bridging structure has been observed previously in the NH_3 and CS emission lines. The ridge resembles the dust envelope of the Sgr A East detected in sub-mm continuum (e.g., Dent et al. 1993, also see figure 11). The southern ridge also has a large velocity gradient along the major axis up to $dV/dr \simeq 2.3$ (km s^{-1} pc^{-1}) (see figure 15b). The velocity gradient is half of that in the northern ridge. The brightness temperature ratio in the southern ridge is as low as two, $R_{\rm SiO/H^{13}CO^+} \simeq 2$. The ratio is, however, increasing with going to the 50-km s^{-1} molecular cloud. The ratio is approximately over three, $R_{\rm SiO/H^{13}CO^+} \gtrsim 3$, near the 50-km s^{-1} molecular cloud. The extension is presumably surrounding the east half of the Sgr A East shell (see figures 9c and 9d).

4.2.3. LVG analysis of SiO emission lines

Here, we estimate the fractional abundance of the SiO molecule, X(SiO), from LVG analysis based on SiO $J = 1$–0

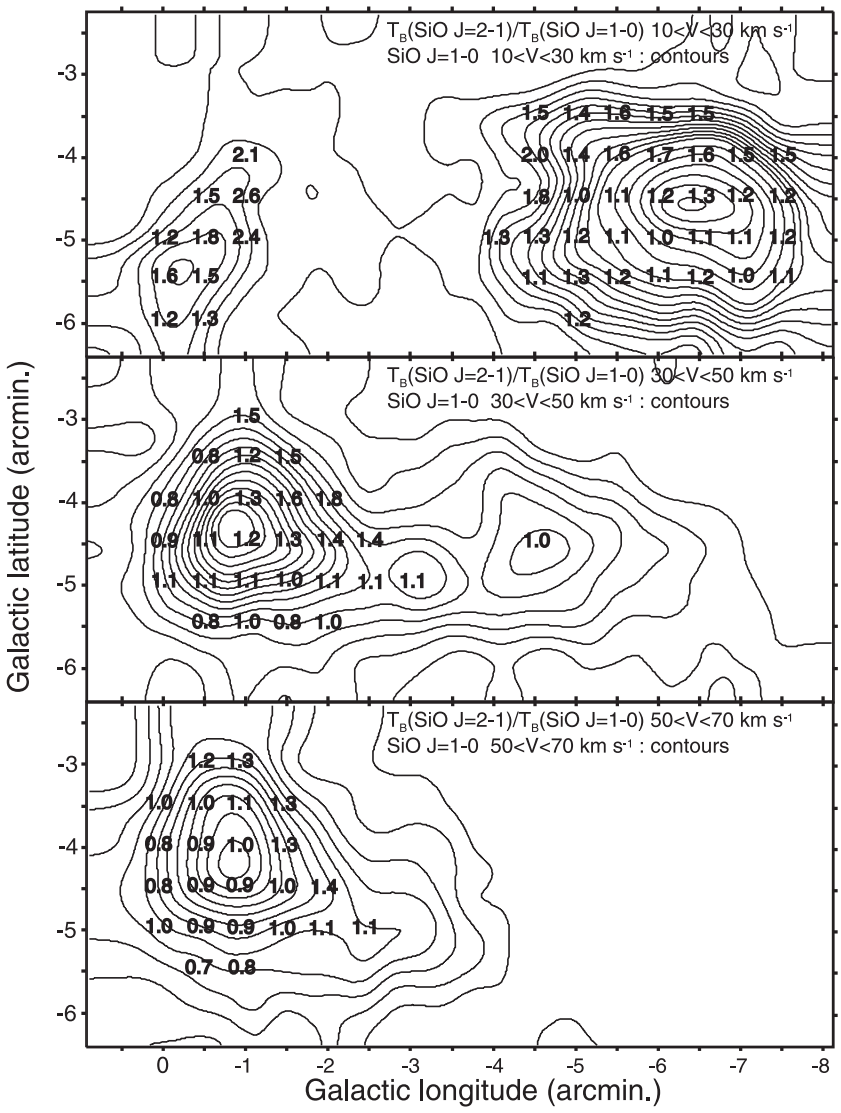

Fig. 16. Distributions of the brightness temperature ratio, $R_{\mathrm{SiO2-1/SiO1-0}} = T_{\mathrm{B}}(\mathrm{SiO}\ J = 2\text{–}1)/T_{\mathrm{B}}(\mathrm{SiO}\ J = 1\text{–}0)$, shown by numbers, which overlay on the velocity-integrated intensity maps in the SiO $J = 1$–0 emission line. The first contour and interval are both $T_{\mathrm{MB}} = 0.10$ K up to $T_{\mathrm{MB}} = 1.20$ K. The interval is $T_{\mathrm{MB}} = 0.20$ K over the value. (Top panel) The velocity range is $V_{\mathrm{LSR}} = 10$–30 km s^{-1}. (Middle panel) The velocity range is $V_{\mathrm{LSR}} = 30$–50 km s^{-1}. (Bottom panel) The velocity range is $V_{\mathrm{LSR}} = 50$–70 km s^{-1}.

and SiO $J = 2$–1 emission-line observations. Figure 16 shows the brightness temperature ratio of the SiO $v = 0$, $J = 1$–0 and SiO $v = 0$, $J = 2$–1 emission lines, $R_{\mathrm{SiO2-1/SiO1-0}} = T_{\mathrm{B}}(\mathrm{SiO}\ J = 2\text{–}1)/T_{\mathrm{B}}(\mathrm{SiO}\ J = 1\text{–}0)$ around Sgr A, overlaid on contour maps of $T_{\mathrm{B}}(\mathrm{SiO}\ J = 1\text{–}0)$. The ratios in the northern half of the 50-km s^{-1} molecular cloud with the velocity range of 10–30 km s^{-1} are slightly higher than 1.5. Others in the 50-km s^{-1} molecular cloud are around unity. Meanwhile, the ratios observed in the 20-km s^{-1} molecular cloud are in the range of 1–2 in the same velocity range. Figure 17a shows the relations based on LVG calculation between SiO $J = 1$–0 brightness temperature, $T_{\mathrm{B}}(\mathrm{SiO}\ J = 1\text{–}0)$, and brightness temperature ratio, $R_{\mathrm{SiO2-1/SiO1-0}}$, on the plane by H_2 number density and SiO fractional abundance per velocity gradient. In this analysis, gas kinetic temperature and background radiation temperature are assumed to be $T_{\mathrm{K}} = 60$ K and $T_{\mathrm{BR}} = 2.73$ K, based on the NH_3 line observation (Miyazaki et al. 2008). Data of the 50-km s^{-1} molecular cloud and the 20-km s^{-1} molecular cloud in figure 16 are shown as filled circles in figure 17, which are heavily scattered. The velocity width of the SiO emission line is also assumed to be 30 km s^{-1} from this observation. From this analysis, $X(\mathrm{SiO})$ in the 50-km s^{-1} molecular cloud and the 20-km s^{-1} molecular cloud is estimated to be $X(\mathrm{SiO}) \simeq 2^{+2}_{-1} \times 10^{-9}$. This SiO fractional abundance is consistent with the values observed in the shocked molecular gas in external galaxies. As mentioned previously, the $H^{13}CO^+$ fractional abundance is $X(H^{13}CO^+) \simeq 1.8 \times 10^{-11}$. The ratio of the fractional abundances of the SiO and $H^{13}CO^+$ molecules is estimated to be $X(\mathrm{SiO})/X(H^{13}CO^+) \sim 1 \times 10^2$ both for the 50-km s^{-1} molecular cloud and the 20-km s^{-1} molecular cloud. The high fractional abundance of SiO and the large velocity width of up to 60 km s^{-1} suggest that

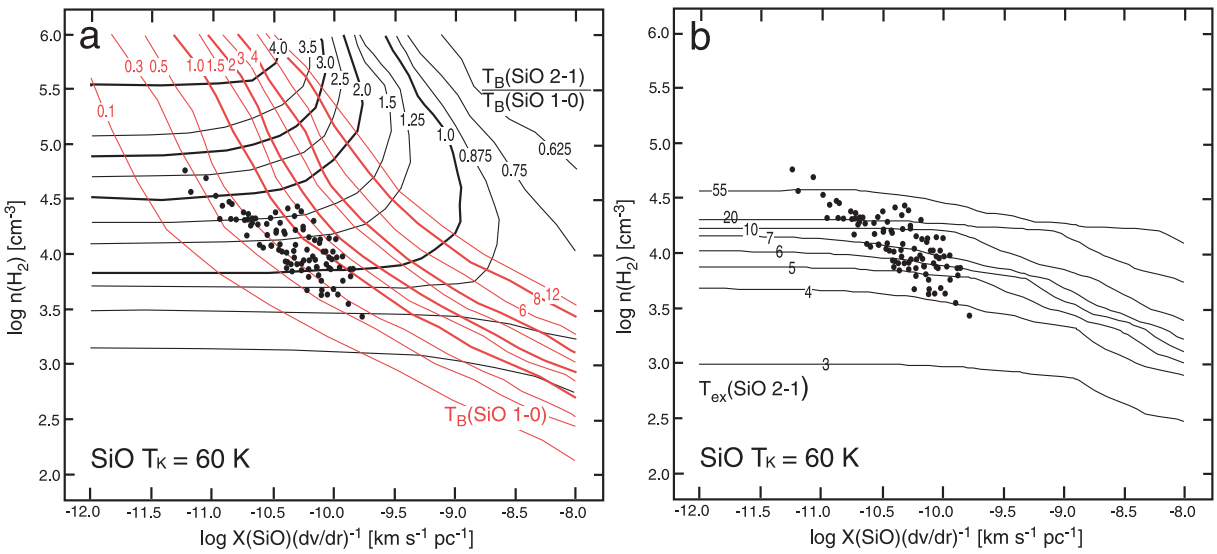

Fig. 17. (a) Relation among H_2 number density, SiO fractional abundance per velocity gradient, SiO $J = 1$–0 brightness temperature, and brightness temperature ratio, $R_{\mathrm{SiO2-1/SiO1-0}} = T_{\mathrm{B}}(\mathrm{SiO}\ J = 2\text{–}1)/T_{\mathrm{B}}(\mathrm{SiO}\ J = 1\text{–}0)$ based on LVG calculation at kinetic temperature of $T_{\mathrm{K}} = 60$ K. Data of the 50-km s^{-1} molecular cloud and the 20-km s^{-1} molecular cloud are shown as filled circles. (b) Excitation temperature of the SiO $J = 2$–1 emission line, $T_{\mathrm{ex}}(\mathrm{SiO}\ J = 2\text{–}1)$, based on LVG calculation at kinetic temperature of $T_{\mathrm{K}} = 60$ K.

these cloud are SiO-enriched by propagation of the C-shock.

Figure 17a also shows that the H_2 density from the LVG analysis of the SiO emission lines is $n_{\mathrm{H_2}} \simeq (0.5\text{–}2) \times 10^4\,\mathrm{cm}^{-3}$ for the 50-km s^{-1} molecular cloud (GCM −0.02−0.07) and the 20-km s^{-1} molecular cloud (GCM −0.13−0.08). The H_2 density is also estimated to be $n_{\mathrm{H_2}} \simeq 2 \times 10^4\,\mathrm{cm}^{-3}$ at $T_{\mathrm{K}} = 60$ K from an LVG analysis based on $C^{32}S$ $J = 1$–0 and $C^{32}S$ $J = 2$–1 observations (e.g., Tsuboi et al. 1999). The derived density is also consistent with the values from the CS observation. In addition, figure 17b shows the excitation temperature of the SiO $J = 2$–1 emission line, $T_{\mathrm{ex}}(\mathrm{SiO}\ J = 2\text{–}1)$, which is based on the LVG calculation. The excitation temperature of the SiO $v = 0$, $J = 2$–1 line is estimated to be $T_{\mathrm{ex}}(\mathrm{SiO}\ J = 2\text{–}1) \sim 4\text{–}20$ K. For the same conditions, except for $X(\mathrm{SiO})/X(\mathrm{H^{13}CO^+}) \sim 1 \times 10^2$, the excitation temperatures of $H^{13}CO^+$ $J = 1$–0 are estimated to be $T_{\mathrm{ex}}(\mathrm{H^{13}CO^+}\ J = 1\text{–}0) \sim 5\text{–}8$ K. This analysis confirmes that the less-abundant molecules, SiO and $H^{13}CO^+$, are clearly sub-thermal in the region.

Assuming that the cloud has a circular orbit, and the large-scale mass distribution around the Galactic center is $M(r) \propto r^{1.2}$ (Sanders & Lowinger 1972), the minimum cloud density required for stability against tidal shear, n_{min}, is given by

$$n_{\mathrm{min}}\,(\mathrm{cm}^{-3}) \sim 2.5 \times 10^7 M_{\mathrm{GC}}(M_\odot)\left[\frac{1}{r(\mathrm{pc})^3} + \frac{1}{r(\mathrm{pc})^{1.8}}\right], \tag{4}$$

where M_{GC} is the mass of the supermassive black hole of the Galactic center, itself, $M_{\mathrm{GC}} = 4 \times 10^6\,M_\odot$, and r is the distance of the cloud from the Galactic center (cf. Güsten & Downes 1980; Stark et al. 1989). If the 20-km s^{-1} molecular cloud is as close as to Sgr A* as the projection on the celestial sphere, the minimum cloud density is $n_{\mathrm{min}} \sim 1 \times 10^5\text{–}3 \times 10^6\,\mathrm{cm}^{-3}$ at $r \sim 4\text{–}20$ pc (0.°03–0.°14). This is much larger than the density from the LVG analysis of the SiO emission lines. An ad hoc excuse is that the real distance of the cloud is much larger than the projected distance. However, this is not plausible because the 20-km s^{-1} molecular cloud must be interacting with CND (e.g., Sato & Tsuboi 2008). Then, a remaining possibility is that the 20-km s^{-1} molecular cloud has been disrupted by tidal shear. The northern ridge of the 20-km s^{-1} molecular cloud is elongated toward Sgr A*, as can be seen in figure 9a. The velocity width is up to 50 km s^{-1} (see figure 15a). These appearances are probably consistent with disruption by tidal shear.

In the case of the 50-km s^{-1} molecular cloud, previous observations pointed out that the cloud is fairly further from Sgr A* than the projection (e.g., Tsuboi et al. 2009). The density from the LVG analysis is much smaller than the minimum cloud density required for stability against the tidal shear at the projection. This is probably consistent with the previous estimated distance of the cloud.

4.3. *Acceleration Spot of Relativistic Electrons Illuminating the Vertical Filaments–Polarized Plumes Complex*

Polarized Plumes are twin linear-polarization-bright components located at both ends of Vertical filaments (Tsuboi et al. 1985, 1986). These form a large scale poloidal magnetic field extending over 150 pc, or the Vertical filaments–Polarized Plumes (Lobes) complex (hereafter, VF–PP). Two unresolved issues remain in VF–PP. First is the origin of such a vertical and long magnetic field. Second is the origin of such abundant relativistic electrons. The later issue means where relativistic electrons are accelerated. In a previous paper based on the CS observation (see figure 7d) (Tsuboi et al. 1997), we proposed that the GCM 0.11−0.11 molecular cloud is colliding with Vertical filaments, and the filaments are probably bending

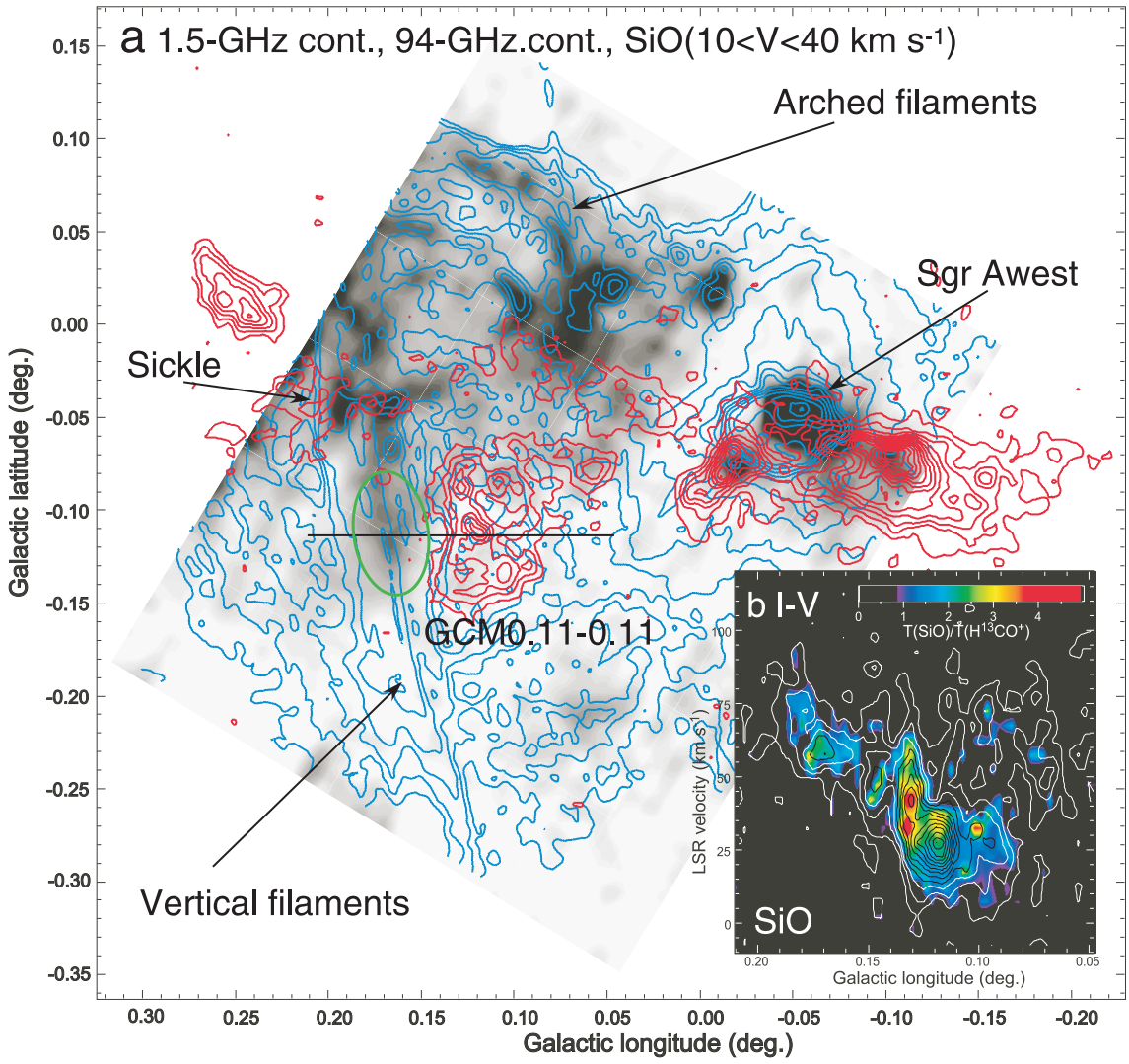

Fig. 18. (a) Velocity-integrated map (red contours) of the Sgr A molecular cloud complex in the SiO $v = 0$, $J = 2$–1 emission line. The velocity range is $V_{\rm LSR} = 15$–45 km s^{-1}. The gray-scale shows an image at 94 GHz observed by the NRO 45-m telescope. Blue contours show an image of Sgr A at 1.5 GHz observed by VLA (Yusef-Zadeh & Morris 1987). The continuum emission feature in a green oval is visible even at 94 GHz although it has no counterpart of thermal and dust emissions. Therefore, this feature is probably synchrotron emission by accelerating relativistic electrons. (b) Galactic longitude–velocity diagram of the GCM 0.11−0.11 molecular cloud in the SiO $v = 0$, $J = 2$–1 emission line along the black line in (a). The first contour and contour interval are both 0.227 K in $T_{\rm MB}$. Pseudo-color shows $T_{\rm B}({\rm SiO})/T_{\rm B}({\rm H^{13}CO^+})$.

at the apparent contact area to the cloud. The collision probably becomes the energy source of the relativistic electrons. If the molecular cloud is really colliding with them, the positive latitude ridge should be more remarkable in the SiO emission line because of shocked molecular gas. Figures 7a and 7c indicate such an expected situation. Figure 18a shows the relation between shocked molecular gas and Vertical filaments. Red contours indicate the distribution of shocked molecular gas by the SiO $v = 0$, $J = 2$–1 emission line. Blue contours are 1.5 GHz continuum emission observed by VLA (Yusef-Zadeh & Morris 1987). The shocked molecular gas in the GCM 0.11−0.11 cloud is visible as a ridge-like structure with a high ratio of $T_{\rm B}({\rm SiO})/T_{\rm B}({\rm H^{13}CO^+})$ up to $\lesssim 4$, and extending parallel to Vertical filaments. Figure 18b shows a Galactic longitude–velocity diagram of the GCM 0.11−0.11 molecular cloud in the SiO $v = 0$, $J = 2$–1 emission line along the black line in figure 18a. The velocity width of the ridge is as large as 70 km s^{-1}, which are four-times larger than those of other clouds in the Galactic center region. The ridge has a high ratio of $T_{\rm B}({\rm SiO})/T_{\rm B}({\rm H^{13}CO^+}) \sim 4$. These features indicate a real interaction between the molecular cloud and the filaments. Relativistic electrons may be accelerated in the magnetic field squeezed with the colliding cloud. The detailed mechanism of the acceleration will be published in other papers.

Meanwhile, the gray-scale image in figure 18a shows 94-GHz continuum emission observed by the NRO 45-m telescope (Tsuboi et al. 2006). This 94-GHz continuum emission indicates not only synchrotron emission from quite high energy relativistic electrons in magnetic field, but also thermal

f–f emission from ionized gas. Although emissions associated with Arched filaments observed at 1.5 GHz should be thermal, a feature around $b \simeq -0.^\circ1$ has no counterpart of thermal and dust emissions (a green oval). This feature is mainly synchrotron emission. This has a peak on the positive longitude side of GCM 0.11−0.11, or $l = 0.^\circ165$, $b = -0.^\circ120$. It seems to be extended along Vertical filaments, $\Delta b \sim 3'$.

The lifetime of the relativistic electrons in magnetic field is given by

$$T_{1/2} = (1/2)C_{12}H^{-3/2}, \tag{5}$$

with the aid of the equipartition condition. Here, C_{12} is a factor depending on the shape of the spectrum and H is the strengh of the magnetic field. We assume that the spectrum between 10 MHz and 100 GHz is flat because this feature is visible at 94 GHz. The lifetime is estimated to be $T_{1/2} = 3 \times 10^3$ yr for $H = 1$ mG. The drift velocity of the relativistic electrons along Vertical filaments must be less than the Alfven velocity, which is given by

$$V_{\rm A}\ ({\rm km\ s^{-1}}) = 2200 \times \frac{H({\rm mG})}{\sqrt{n_{\rm H}({\rm cm^{-3}})}}. \tag{6}$$

The drift length of relativistic electrons emitting at 94 GHz is less than $l_{\rm D} = V_{\rm A} \times T_{1/2} \leq 7/\sqrt{n_{\rm H}}$ pc within the lifetime. The observed size of this feature is consistent with the drift length of the relativistic electrons, $l_{\rm D}$. This presumably shows that the relativistic electrons are accelerated here in the filaments. Also, they are presumably drifting to north and south along the filaments. In addition, previous observations show that the spectral index, α, along VF–PP ($S_\nu \propto \nu^{-\alpha}$) is decreasing with increasing distance from $b \simeq -0.^\circ1$ (Tsuboi et al. 1995). The small size of the 94 GHz emitting area around $b \simeq -0.^\circ1$ is a supporting evidence of the hypothesis that the cloud impacts with Vertical filaments.

5. Conclusions

We have performed a high-resolution wide-field mapping observation of the Sgr A molecular cloud complex in the $H^{13}CO^+$ $J = 1$–0 and SiO $v = 0$, $J = 2$–1 emission lines using the Nobeyama Radio Observatory 45-m telescope. The effective angular resolution is 26″. The molecular clouds in the $H^{13}CO^+$ emission line presents clumpy and/or filamentary structures, although the line is optically thin and is not emphasized by shock, even in the Galactic center region. We estimated the fractional abundance in the Sgr A complex to be $N(H^{13}CO^+)/N_{H_2} \simeq 1.8 \times 10^{-11}$ compared with the virial theorem mass and the hydrogen mass by sub-millimeter continuum data. Many molecular clouds are remarkable only in the SiO emission line, which is a tracer of shocked molecular gas. These molecular clouds have an arc-like appearance and a large velocity width of up to 60 km s^{-1}. The brightness temperature ratio is up to $T_{\rm B}({\rm SiO})/T_{\rm B}(H^{13}CO^+) \lesssim 8$. The features are dominated by shock SiO-enriched gas. In such clouds, the ratio of the fractional abundance of the SiO and $H^{13}CO^+$ molecules is $X({\rm SiO})/X(H^{13}CO^+) \gtrsim 1 \times 10^2$. The high brightness temperature ratio indicates an expanding shell in the 50-km s^{-1} molecular cloud. This feature is presumably made by an SNR embedded in the cloud. There is a wide-velocity width ridge of SiO-enriched gas in GCM 0.11−0.11, which is adjacent to Vertical filaments. This suggests that the collisions with the molecular cloud accelerate relativistic electrons, which illuminate the Vertical filaments–Polarized Plumes complex.

The authors would like to thank the members of the 45-m telescope group of Nobeyama Radio Observatory for support in the observations. They also thanks M.T. Sato of the University of Tokyo for useful discussion.

References

Amo-Baladrón, M. A., Martín-Pintado, J., Morris, M. R., Muno, M. P., & Rodríguez-Fernández, N. J. 2009, ApJ, 694, 943
Bally, J., Stark, A. A., Wilson, R. W., & Henkel, C. 1987, ApJS, 65, 13
Dent, W. R. F., Matthews, H. E., Wade, R., & Duncan, W. D. 1993, ApJ, 410, 650
Dowell, C. D., Lis, D. C., Serabyn, E., Gardner, M., Kovacs, A., & Yamashita, S. 1999, in ASP Conf. Ser., 186, The Central Parsecs of the Galaxy, ed. H. Falcke et al. (San Francisco: ASP), 453
Güsten, R., & Downes, D. 1980, A&A, 87, 6
Handa, T., Sakano, M., Naito, S., Hiramatsu, M., & Tsuboi, M. 2006, ApJ, 636, 261
Herrnstein, R. M., & Paul, P. T. P. 2005, ApJ, 620, 287
Ho, P. T. P., Jackson, J. M., Barrett, A. H., & Armstrong, J. T. 1985, ApJ, 288, 575
Ikeda, N., Sunada, K., & Kitamura, Y. 2007, ApJ, 665, 1194
Lis, D. C., & Carlstrom, J. E. 1994, ApJ, 424, 189
Mauersberger, R., & Henkel, C. 1991, A&A, 245, 457
Milam, S. N., Savage, C., Brewster, M. A., Ziurys, L. M., & Wyckoff, S. 2005, ApJ, 634, 1126
Miyazaki, A., & Tsuboi, M. 2000, ApJ, 536, 357
Miyazaki, A., Tsuboi, M., & Handa, T. 2008, PASJ submitted
Morris, M., & Serabyn, E. 1996, ARA&A, 34, 645
Oka, T., Hasegawa, T., Sato, F., Tsuboi, M., & Miyazaki, A. 1998, ApJS, 118, 455
Okumura, S. K., et al. 1989, ApJ, 347, 240
Pedlar, A., Anantharamaiah, K. R., Ekers, R. D., Goss, W. M., van Gorkom, J. H., Schwarz, U. J., & Zhao, J.-H. 1989, ApJ, 342, 769
Pierce-Price, D., et al. 2000, ApJ, 545, L121
Poglitsch, A., Stacey, G. J., Geis, N., Haggerty, M., Jackson, J., Rumitz, M., Genzel, R., & Townes, C. H. 1991, ApJ, 374, L33
Sanders, R. H., & Lowinger, T. 1972, AJ, 77, 292
Sato, M. T., & Tsuboi, M. 2008, J. Phys. Conf. Ser., 131, 012033
Sawada, T., et al. 2008, PASJ, 60, 445
Serabyn, E., & Güsten, R. 1987, A&A, 184, 133
Sjouwerman, L. O., Pihlström, Y. M., & Fish, V. L. 2010, ApJ, 710, L111
Stark, A. A., Bally, J., Wilson, R. W., & Pound, M. W. 1989, in IAU Symp.136, The Center of the Galaxy, ed. M. Morris (Dordrecht: Kluwer Academic Publishers), 129
Stolovy, S., et al. 2006, J. Phys. Conf. Ser., 54, 176
Sunada, K., Yamaguchi, C., Nakai, N., Sorai, K., Okumura, S. K., & Ukita, N. 2000, Proc. SPIE, 4015, 237

Tsuboi, M., Handa, T., & Ukita, N. 1999, ApJS, 120, 1
Tsuboi, M., Inoue, M., Handa, T., Tabara, H., & Kato, T. 1985, PASJ, 37, 359
Tsuboi, M., Inoue, M., Handa, T., Tabara, H., Kato, T., Sofue, Y., & Kaifu, N. 1986, AJ, 92, 818
Tsuboi, M., Kawabata, T., Kasuga, T. Handa, T., & Kato, T. 1995. PASJ, 47, 829
Tsuboi, M., Miyazaki, A., & Handa, T. 2006, in Mapping the Galaxy and Nearby Galaxies, ed. K. Wada & F. Combers (New York: Springer), 133
Tsuboi, M., Miyazaki, A., & Okumura, S. K. 2009, PASJ, 61, 29
Tsuboi, M., Tadaki, K., Sato, T. M., Miyazaki, A., & Handa, T. 2011, Proc. the Galactic Center: a Window to the Nuclear Environment of Disk galaxies 2009, ed. M. Morris et al. (San Fransisco: ASP), 23
Tsuboi, M., Ukita, N., & Handa, T. 1997, ApJ, 481, 263
Yusef-Zadeh, F., Law, C., & Wardle, M. 2002, ApJ, 568, L121
Yusef-Zadeh, F., & Morris, M. 1987, ApJ, 320, 545
Yusef-Zadeh, F., Morris, M., & Chance, D. 1984, Nature, 310, 557
Yusef-Zadeh, F., Stdovy, S. R., Burton, M., Wardle, M., & Ashley, M. C. B. 2001 ApJ, 560, 749
Ziurys, L. M., Friberg, P., & Irvin, W. M. 1989, ApJ, 343, 201